Bioactive Materials 43 (2025) 423–440

Contents lists available at ScienceDirect

Bioactive Materials

journal homepage: www.keaipublishing.com/en/journals/bioactive-materials

Hydrogel microsphere stem cell encapsulation enhances cardiomyocyte differentiation and functionality in scalable suspension system

Mohammadjafar Hashemi [a], Ferdous B. Finklea [a], Hanna Hammons [a], Yuan Tian [a], Nathan Young [a], Emma Kim [a], Caroline Halloin [b], Wiebke Triebert [b], Robert Zweigerdt [b], Amit Kumar Mitra [c], Elizabeth A. Lipke [a,*]

[a] Department of Chemical Engineering, Auburn University, Auburn, AL, United States
[b] Leibniz Research Laboratories for Biotechnology and Artificial Organs (LEBAO), Department of Cardiothoracic, Transplantation and Vascular Surgery, Hannover Medical School, Hanover, Germany
[c] Department of Drug Discovery and Development, Harrison College of Pharmacy, Auburn University, Auburn, AL, United States

ARTICLE INFO

Keywords:
Human induced pluripotent stem cells
Suspension culture
Scale-up
Chemically defined media
Aggregate formation
PEG-fibrinogen

ABSTRACT

A reliable suspension-based platform for scaling engineered cardiac tissue (ECT) production from human induced pluripotent stem cells (hiPSCs) is crucial for regenerative therapies. Here, we compared the production and functionality of ECTs formed using our scaffold-based, engineered tissue microsphere differentiation approach with those formed using the prevalent scaffold-free aggregate platform. We utilized a microfluidic system for the rapid (1 million cells/min), high density (30, 40, 60 million cells/ml) encapsulation of hiPSCs within PEG-fibrinogen hydrogel microspheres. HiPSC-laden microspheres and aggregates underwent suspension-based cardiac differentiation in chemically defined media. In comparison to aggregates, microspheres maintained consistent size and shape initially, over time, and within and between batches. Initial size and shape coefficients of variation for microspheres were eight and three times lower, respectively, compared to aggregates. On day 10, microsphere cardiomyocyte (CM) content was 27 % higher and the number of CMs per initial hiPSC was 250 % higher than in aggregates. Contraction and relaxation velocities of microspheres were four and nine times higher than those of aggregates, respectively. Microsphere contractile functionality also improved with culture time, whereas aggregate functionality remained unchanged. Additionally, microspheres displayed improved β-adrenergic signaling responsiveness and uniform calcium transient propagation. Transcriptomic analysis revealed that while both microspheres and aggregates demonstrated similar gene regulation patterns associated with cardiomyocyte differentiation, heart development, cardiac muscle contraction, and sarcomere organization, the microspheres exhibited more pronounced transcriptional changes over time. Taken together, these results highlight the capability of the microsphere platform for scaling up biomanufacturing of ECTs in a suspension-based culture platform.

1. Introduction

Due to the current limited supply of human cardiac tissue and the inability of adult cardiomyocytes (CMs) to be expanded in culture, the development of advanced *in-vitro* platforms capable of generating functional human cardiomyocytes and engineered cardiac tissue (ECT) is crucial for advancing cardiac regeneration [1], drug discovery [2], cardiotoxicity testing [3], and disease modeling [4]. Human-induced pluripotent stem cells (hiPSCs) are a promising candidate for large-scale production of hiPSC-derived CMs (hiPSC-CMs) [5]. However, production of clinically relevant quantities of hiPSC-CMs in cost-effective and xenobiotic-free (xeno-free) media is challenging, especially given the low or fluctuating differentiation efficiency in suspension culture [6,7] and the incomplete functional maturation of resulting hiPSC-CMs [8–10].

While two-dimensional (2D) hiPSC cardiac differentiation is efficient and reproducible [11], due to the substantial surface area required, this approach faces limitations in scalability to meet the demand for clinical

Peer review under responsibility of KeAi Communications Co., Ltd.
* Corresponding author.
E-mail address: elipke@auburn.edu (E.A. Lipke).

https://doi.org/10.1016/j.bioactmat.2024.08.043
Received 18 April 2024; Received in revised form 30 August 2024; Accepted 31 August 2024

and commercial hiPSC-CMs [12,13]. Thus, there is a compelling need for a three-dimensional (3D) suspension-based scalable platform for hiPSC expansion and differentiation to CMs, as reviewed by H Kempf et al. [14] and CK Kwok et al. [15]. 3D hiPSC cardiac differentiation platforms can be classified into scaffold-free and scaffold-supported approaches. In scaffold-free systems, the aim is to create 3D self-aggregated tissues without relying on biomaterials, thereby avoiding dependence on a provided matrix or substrate. Approaches such as hanging droplets [16], the forced-floating method [17], and ultra-low attachment well plates [18] have been employed to achieve this. On the other hand, scaffold-based approaches involve the integration of cells with biomaterial scaffolds, such as microcarriers [19–21], as well as natural and synthetic biomaterials, and other types of polymers [22–24]. By leveraging the inherent properties of these biomaterial scaffolds and fine-tuning the microenvironmental properties, the viability and differentiation of stem cells can be effectively promoted [25].

A common scaffold-free biomanufacturing strategy employed for the scalable production of hiPSC-CMs includes inducing the self-aggregation of a single-cell suspension of hiPSCs within a stirred tank or shaker flask system; this process is referred to as "aggregate" differentiation. This approach offers some advantages over scaffold-supported systems, including promoting a bottom-up strategy that allows for the creation of tissue constructs with higher cell density and better cell-to-cell interactions [26]. However, suspension-based, scaffold-free systems present challenges in efficiently modulating key parameters essential for optimizing both stem cell expansion and differentiation, including aggregate size [21], shape [27], number of cells per aggregate [28], and formation kinetics [29]. The inherent limitations in controlling these factors contribute to the observed batch-to-batch variations in cardiac differentiation [30]. The pattern of stem cell aggregate formation in the expansion phase has been demonstrated to affect cardiac differentiation, with hiPSC-CM contents ranging from 26 to 90 % in a bioreactor [31]. Controlling aggregate size and cellular microenvironment in suspension culture can be accomplished through external manipulations [32]; this approach alters hydrodynamic forces which can potentially impact stem cell phenotype and differentiation [29,33,34]. To provide tighter, more direct control and improve hiPSC-CMs functionality, multiple approaches have been tested, including employing biomaterial supports such as microcarriers [35], pre-formed scaffolds [36], and hydrogel matrices [37].

Integration of hiPSCs into a tunable hydrogel matrix microenvironment has the potential to enhance initial size and shape uniformity, CM yield, batch-to-batch cardiac differentiation consistency, establish a homogeneous cellular microenvironment, and guide stem cell differentiation. Furthermore, this encapsulation strategy offers protection against the shear stresses inherent in suspension-based cultures, facilitates precise control over initial cell density, and provides cues to guide stem cell differentiation [29]. Our prior work [37–40], as well as contributions of other researchers [3,41], has demonstrated the ability of hiPSC-laden hydrogels to support cardiac differentiation of the encapsulated hiPSCs. To facilitate the scaled-up production of hiPSC-CMs, we previously employed a novel microfluidic system [40] to rapidly encapsulate hiPSCs within poly(ethylene glycol)-fibrinogen (PEG-fibrinogen, PF) hydrogel microspheres prior to cardiac differentiation [37]. However, to evaluate whether scale-up of this approach in a clinically applicable system incorporating chemically defined media is worth pursuing, additional studies with direct comparison to self-aggregation approaches are required to assess the effects of providing a hydrogel matrix to hiPSCs.

We hypothesized that by providing an initial spheroid-engineered microenvironment for hiPSCs, we could reduce size and shape variability within and between batches, enhance cell production and improve efficiency in CM differentiation, and alter contractile functionality and structural maturation of hiPSC-CMs. Although prior work has demonstrated the ability of biomaterials to support cardiac differentiation in suspension, direct comparison of these approaches to aggregate-based differentiation is needed. Therefore, in this study, we evaluate, for the first time, the effects on hiPSCs encapsulated within a PF hydrogel and hiPSC aggregates during cardiac differentiation in chemically defined media, which is amenable to scale-up.

In this study, through a direct comparison between the microsphere (MS) and aggregate (Agg) differentiation platforms, we examine the previously uninvestigated effects of stem cell encapsulation on cellular behavior and cardiac differentiation outcomes. To rapidly produce uniform microspheres, we utilized a microfluidic system [42]. For aggregate formation, a single-cell suspension was agitated in a shaker flask [43] on an orbital shaker, a technique commonly employed for scale-up studies prior to stirred-tank bioreactor experiments. Cardiac tissues formed using the microsphere differentiation platform exhibited higher uniformity of initial size and shape within and across batches. Additionally, these tissues displayed higher content and yield of CMs, enhanced contractile functionality, and a more pronounced responsiveness to isoproterenol and propranolol, in comparison to aggregates that underwent a similar differentiation process. This showcases the potential to augment the uniformity, yield, and functionality of cardiac tissue generated by encapsulating hiPSCs within PF in scalable suspension culture systems.

2. Materials and methods

2.1. HiPSC culture

The hiPSC cell lines, IMR-90 Clone 1 (WiCell) and Un-Arc 16 Facs II [44], were cultured on Matrigel (Corning) with mTeSR-1 medium (Stem Cell Technologies) and on Geltrex (Gibco)-coated T-25 flasks in Essential E8 medium, respectively, as previously described [45]. Briefly, hiPSCs were passaged every three days using Accutase (Innovative Cell Technologies) for Un-Arc 16 Facs II and Versene (Invitrogen) for IMR-90. Following passaging, hiPSCs were maintained in E8 medium supplemented with ROCK inhibitor (5–10 μM, Y 27632, Stem Cell Technologies) for 24 h.

2.2. PEG-fibrinogen (PF) synthesis

All chemicals were purchased from Sigma-Aldrich unless specified otherwise. First, poly(ethylene glycol)-diacrylate (PEGDA) was synthesized by acrylating PEG (10 kDa) as described previously [46]. PF, a hybrid biomaterial currently undergoing clinical trials for cartilage tissue repair [47], was synthesized as previously described [48,49]. Briefly, bovine fibrinogen (Type I-S; Sigma) was covalently coupled to PEGDA. Fibrinogen (7 mg/mL) was dissolved in a phosphate buffered saline (PBS) solution containing 8 M urea (Sigma), with the pH adjusted to 7.4. Next, tris (2-carboxyethyl) phosphine hydrochloride (TCEP-HCl) (Acros Organics) was added to the solution. PEGDA was dissolved in 280 mg/mL of urea-PBS at room temperature. Then, dissolved PEGDA was slowly added to the fibrinogen solution to react for 3 h in the dark at ambient temperature. To stop the reaction, an equal volume of 8M urea-PBS was mixed, and then acetone at a 4:1 volumetric ratio was added to precipitate the reaction products. After centrifuging and removing the acetone, the product was weighed and dissolved in 8M urea-PBS at a concentration of 2.2 mL of buffer per gram of product. The product was dialyzed against PBS at 4 °C in the dark overnight and stored at −80 °C. To characterize the PEGylated product, fibrinogen content was measured using Pierce BCA assay (Thermo Scientific).

2.3. HiPSC microsphere encapsulation

To produce hydrogel microspheres, a novel microfluidic system with a custom-developed polydimethylsiloxane (PDMS) mold was used as previously described [42]. Briefly, the PDMS mold was created by combining Sylgard 184 silicone elastomer and Sylgard 184 curing agent (Dow Corning) and pouring it into a preassembled frame made with a

glass bottom, an acrylonitrile butadiene styrene (ABS) plastic bracket, and spacers held by the bracket to form the channels within the PDMS mold. Then, the air bubbles were removed by a vacuum. PDMS molds were sterilized by sonication in 70 % ethanol before and after each use.

To encapsulate hiPSCs, the PF polymer precursor solution was prepared using PF at a final protein concentration of about 12 mg/mL in phosphate buffered saline (PBS). The PF was combined with 1.5v/v% triethanolamine (TEOA) (Acros Organics) as co-initiator, 0.4v/v% N-vinylpyrrolidone (NVP) (Sigma) as comonomer, and 1 v/v% Eosin Y (Fischer Scientific) as visible light photoinitiator. HiPSCs were resuspended in PF precursor solution at a concentration of 30, 40, and 60 million hiPSCs mL^{-1} using a wide orifice pipette tip. The precursor solution was infused into the top inlet of the mold, and the mineral oil was pumped from the bottom up to break the surface tension of the precursor solution and form microspheres. In the outlet channel, the cell-laden microspheres were crosslinked using a 2.7 W visible light, resulting in a cell encapsulation rate of one million cells per minute. The microspheres were washed down with E8 medium supplemented with 10 μM Y-27632 (ROCK inhibitor, RI) at the end of the PDMS mold. The microspheres were cultured in E8 medium supplemented with 10 μM RI for 24 h (day −3) on a 6-well plate at 37 °C and 5 % CO_2. The media was changed every day using fresh E8 until day 0.

2.4. 3D self-aggregate (aggregate) formation

Scaffold-free self-aggregates (referred to as 'aggregates') were generated by culturing hiPSCs in either a shaker flask or a well plate, as previously described [43,50]. To initiate aggregate formation, hiPSCs were detached from a tissue culture flask using Accutase (Innovative Cell Technologies), and the resulting cell pellet was suspended in E8 medium supplemented with 10 μM RI. This cell suspension was then placed on an orbital shaker plate (Infors) at 70 rpm on day −3. Daily media changes were carried out using fresh E8 medium leading up to the commencement of cardiac differentiation. The differentiation process for both microspheres (MS) and aggregates (Agg) is elaborated upon in the subsequent section. Additionally, three distinct platforms were utilized for aggregate seeding and differentiation: these encompassed seeding and differentiation within a shaker flask (referred to as 'F'), seeding and differentiation within a well plate (referred to as 'P'), and a hybrid approach involving seeding in a shaker flask and subsequent differentiation within a well plate (referred to as 'F/P').

2.5. Cardiac differentiation

Cardiac differentiation for both microspheres (MS) and self-aggregates (Agg) was initiated on day 0 following a well-established protocol [43]. In the shaker flask platform, 3 million hiPSCs were seeded, and the total number of cells on day 0 was used for differentiation without adjusting the cell density, i.e. cells per volume of media. The well plate platform was similar in that the number of cells on day 0 was used for differentiation without any adjustments prior to initiation of differentiation with chemically defined medium containing three components (CDM3) [51] supplemented with CHIR99021 (Stem Cell Technologies). For the F/P platform, 3 million cells were seeded in the shaker flask and on day 0, the cells were collected, a sample was counted, and the remaining aggregate were distributed to provide 0.5 million hiPSCs mL^{-1} cell density on day 0 and provide a similar microenvironment as the microspheres.

The number of cells on day 0 was counted by dissociating the microspheres, and the cell density in each well of a 6-well plate was set at 0.5 million hiPSCs mL^{-1} CDM3 before starting the differentiation. E8 medium was replaced with CDM3 [51] medium supplemented with 5 μM CHIR99021 for the Un-Arc 16 Facs II cell line and 7.5 μM for the IMR-90 cell line, and the well plate was placed on the shaker plate (Infors) on day 0. Precisely 24 h later (day 1), the medium was replaced with a CDM3 medium, which was supplemented with 5 μM IWP2 (Stem Cell Technologies). After 48 h (day 3), the media was replaced with 4 mL of fresh CDM3. The medium was changed every other day until day 7 and replaced with RPMI/B27 containing insulin (Invitrogen) on day 10. For long-term culturing, the media was changed every three days with RPMI/B27 containing insulin.

2.6. Microspheres and aggregates geometry characterization

Microspheres exhibit autofluorescence due to the presence of the Eosin Y photoinitiator (Fisher Scientific). To assess the uniformity, initial size, and shape of the microspheres and aggregates, fluorescence and phase-contrast images were captured at the earliest possible time point for each system: on day −2 for microspheres and on day 0 for aggregates (using a Ti Eclipse microscope, Nikon, equipped with an Andor Luca S camera) (Supplementary Fig. 1). Microsphere size and shape are established through the encapsulation process on day −3. To avoid interfering with the aggregate formation process, aggregates were imaged on day 0, following their full formation from single cells seeded on day −3. At least 30 microspheres and 30 aggregates from each of seven separately prepared batches of microspheres and aggregates were measured using ImageJ. Diameter as size and axial ratio (AR), which is a ratio between axis, as shape were analyzed by manual outlining of microspheres using Bio-format plugin ImageJ (version 2.3.0/1.53q). Microsphere and aggregate growth area prior to the initiating of spontaneous contraction was determined. Phase contrast images were taken on day 0, 1, 3, 5, and 7 of differentiation for four separate batches. A minimum of 30 microspheres and aggregates per batch were measured using ImageJ.

2.7. Tissue dissociation and 2D re-plating

Microspheres and aggregates were incubated in a dissociation solution consisting of Collagenase-B (1 mg/mL, Roche) supplemented with DNase (0.05 mg/mL, Worthington) in PBS. The incubation took place at 37 °C for 2 min with shaking, followed by 2 min of resting time. This was then followed by gentle pipetting, limited to a maximum of three times. After completely dissociating, the cells were centrifuged for 3 min at 300 g, resuspended in RPMI 20 medium (RPMI 1640 medium with 20 % fetal bovine serum (FBS, Atlanta Biologicals) supplemented with 5 μM RI, and seeded on a Matrigel-coated coverslip for two days before starting staining.

2.8. HiPSC viability and immunofluorescent visualization

The impact of the encapsulation process and single-cell suspension culture of aggregates on hiPSC viability was examined using a LIVE/DEAD viability kit (Invitrogen) following the manufacturer's protocol. Subsequently, images were acquired using a confocal microscope (Nikon).

Immunofluorescence staining was executed to visualize protein expression. Whole or dissociated cell-laden microspheres and aggregates were subjected to staining with Alexa Fluor 568 phalloidin (actin filaments, Invitrogen, 1:1000), Ki67 (Abcam, 1:300), Oct4 (Abcam, 1:300), α-sarcomeric actinin (αSA Mouse, Sigma Aldrich, 1:400), cardiac troponin T (cTnT Mouse IgG, Invitrogen, 1:400), Mito Tracker Red (Invitrogen, 1:1000), Collagen I (Rabbit IgG, Rockland, 1:200), and connexin 43 (Cx43 Rabbit IgG, Sigma Aldrich, 1:100). For staining of whole microspheres and aggregates (phalloidin, Ki67, Oct4, Collagen I, cTnT, with the same dilution mentioned above), the samples were rinsed with PBS and fixed in 4 % paraformaldehyde (Electron Microscopy Sciences) for 30 min at ambient temperature on a Boekel Scientific 260250 Orbitron Rotator. Phalloidin and Hoechst were utilized to stain F-actin and nuclei, respectively. Cells were permeabilized by adding PBS-T (PBS with 1 % (w/v) bovine serum albumin (BSA) and 0.2 % (v/v) TritonX-100) to the sample twice for 30 min each at ambient temperature on the rotator. Subsequently, the samples were blocked using a 10

% FBS in PBS blocking buffer for 1 h at room temperature. For microspheres and aggregates, the primary antibodies (Ki67, Oct4, Collagen I, cTnT) were applied overnight at 4 °C. Secondary antibodies Alexa Fluor 488 and 647 were employed for detection.

For staining dissociated hiPSC-CMs on Matrigel-coated coverslips (Mito Tracker Red, αSA, connexin 43), the samples underwent a PBS wash supplemented with potassium chloride (KCl) (Sigma) to induce relaxation of the cardiomyocytes. A working solution of Mito Tracker Red was introduced into the medium (1:1000) for a 30-min incubation at 37 °C. Subsequently, cells were fixed using 4 % and 2 % paraformaldehyde (PFA) (Electron Microscopy Sciences) at room temperature for 20 min to enable mitochondria and connexin 43 immunostaining, respectively. Post-fixation, cells were subjected to two rounds of PBS washes followed by permeabilization using PBS-T containing 0.2 % Triton X-100 in PBS for 30 min. Blocking was then achieved by treating cells with 10 % FBS in a PBS blocking buffer for 45 min at room temperature. Incubation with primary antibodies (αSA and Cx43, with the same dilution mentioned above) took place overnight at 4 °C. After four subsequent PBS-T washes, each lasting 5 min, cells were incubated in the secondary antibodies (Alexa Fluor 568 and 488, 1:200) along with Bisbenzimide Hoechst 3342 (MilliporeSigma) for 1 h at room temperature. To prepare the samples for visualization, a dehydration process was executed using ethanol concentrations of 50 %, 75 %, 95 %, and 100 % each lasting 5 min. Following this, samples were air-dried, and a small drop of ProLong Gold was applied to a rectangular glass coverslip. The sample was then inverted onto the glass. After overnight drying and sealing with nail polish, the samples were stored at 4 °C and subsequently visualized using a Nikon Eclipse TE2000 Inverted Microscope equipped with a Nikon A1 plus Confocal Microscope System.

2.9. Evaluation of hiPSC-CMs cell morphology and sarcomere structure

To comprehensively assess hiPSC-CMs cell morphology and sarcomere structure, immunofluorescent confocal images of dissociated and re-plated microspheres and aggregates on days 20 and 30 were captured. For automated segmentation and texture analysis, an unbiased algorithm, SarcOmere Texture Analysis (SOTA) [52], was adapted and modified. For accurate measurement of sarcomere length, we incorporated a second MATLAB algorithm, SarcTrack, developed by Toepfer et al. [53], into the SOTA code. Since these codes were developed for analyzing monolayer cardiomyocytes, we adapted this approach to our study by dissociating the microspheres and aggregates, as previously described, and replating them on a 2D surface. We then performed immunostaining using αSA (at the same dilution mentioned above) and Bisbenzimide Hoechst 3342 (MilliporeSigma).

2.10. Characterization of mitochondria

To characterize the mitochondria, immunofluorescent confocal images of dissociated hiPSC-CMs from both microsphere and aggregate platforms on day 30 were acquired. A previously described MATLAB code [54] was employed to analyze the images and extract relevant information.

2.11. Contraction analysis of microspheres and aggregates

The spontaneous contraction of intact microspheres was recorded on days 10 and 20 (n = 10 individual microspheres for each batch at each time point). Likewise, the contraction of complete aggregates was recorded on day 10 and day 15+ (n = 10 individual aggregates for each batch at each time point). Subsequent to converting videos into a series of TIFF images, motion analysis between the images was conducted through the utilization of a MATLAB code [55]. To plot the frequency of contraction, time interval, the average maximum contraction, and the relaxation velocities, the “Data Evaluation” interface was employed.

2.12. Flow cytometry

Flow cytometry was performed on cells between day 9–13 of differentiation. Following dissociation, cells were washed with PBS and unlabeled samples were collected. Subsequently, the cells were subjected to incubation with Zombie dye (Biolegend) (1:1000) in the dark at 4 °C for 30 min. Meanwhile, a cell sample was counted. The cells were washed with a blocking buffer (1 % BSA and 10%FBS in 1x PBS) and then fixed and permeabilized using cold Foxp3 Fixation/Permeabilization (ThermoFisher) working solution overnight at 4 °C. Permeabilization Buffer (Invitrogen) was introduced to the cells. Supernatant was aspirated, and the cells were incubated with FACS buffer for 30 min. After filtering, cells were labeled with primary antibodies (cTnT, Invitrogen, 1:800; aSA, AbCam, 1:400; MF20, Developmental Studies Hybridoma Bank, The University of Iowa, 1:200; IgG Isotype, ThermoFisher, 1:1000) diluted in FACS buffer (100 μL). Incubation took place for 1 h at room temperature, followed by two washes with Permeabilization Buffer before adding secondary antibody (Alexa Fluor 647, Invitrogen, 1:300) diluted in FACS buffer (100 μL). Subsequently, cells were incubated for 45 min. Following additional washing steps, samples were analyzed utilizing a CytoFLEX LX flow cytometer (Beckman Coulter).

2.13. Electrophysiological characterization and drug response

To visualize calcium propagation, optical mapping was performed by using a high-speed camera (Andor iXon+ 860 EMCCD) mounted on a fluorescent microscope (Ti Eclipse Nikon), utilizing our established optical mapping system as previously described [56]. The whole microspheres and aggregates were stained with the calcium dye Rhod-2 (Invitrogen) on day 20. A dye solution was prepared by combining 0.5 μM Rhod-2 with RPMI B27 containing blebbistatin (50 μM, Sigma) to uncouple fluorescent motion related to Ca^{2+} propagation from motion-related fluorescent signals. The whole microspheres and aggregates ($n \geq 3$ tissues) were incubated in the dye solution for a duration of 2 h at 37 °C. Subsequently, the tissues were washed and transferred to Tyrode’s solution (containing 1.8 mM $CaCl_2$, 5 mM glucose, 5 mM HEPES, 1 mM $MgCl_2$, 5.4 mM KCl, 135 mM NaCl, and 0.33 mM NaH_2PO_4, pH 7.4) within an optical mapping chamber at 37 °C. Videos were recorded and analyzed through a custom MATLAB script. This script utilized changes in fluorescence to determine parameters such as calcium transient duration (CTD) at 50 and 80 percent repolarization, frequency, and conduction velocity (CV).

The ability of hiPSC-CMs to respond adequately to pharmacological stimulation from β-adrenergic agonist (isoproterenol- Iso) and antagonist (propranolol- Pro) was examined in both platforms. Spontaneously contracting microspheres and aggregates were exposed to isoproterenol (Molecular Devices) and propranolol (Molecular Devices). In a sequential manner, isoproterenol (1 μM) was first added to the microspheres and aggregates, followed by the subsequent introduction of 1 μM propranolol. Subsequently, the drugs were washed out to attain baseline contraction frequencies. Videos were taken before and after incubating the samples in the drugs, and the frequency of contraction was analyzed using the open-source MATLAB code [55].

2.14. RNA extraction and next-generation RNA sequencing (NGS)

High-quality RNA was isolated using QIAshredder columns and RNeasy kit (Qiagen). RNA concentration and RNA integrity were assessed using Nanodrop-8000 and Agilent 2100 Bioanalyzer and stored at −80 °C. An RNA integrity number (RIN) threshold of 8 was applied and RNA-seq libraries were constructed using Illumina TruSeq RNA Sample Preparation Kit v2. NGS Libraries were size-selected and RNA sequencing was performed on Illumina’s NovaSeq 6000 platform using 150 bp paired-end protocol with a depth of >20 million reads-per-sample.

2.15. RNAseq data analysis

Genome wide RNA expression data was pre-processed, log2-transformed, and analyzed using a combination of command line-based analysis pipeline, and Partek Flow software to identify differential gene expression profiling (GEP) signatures. The data have been archived in the NCBI Gene Expression Omnibus repository under GEO ID GSE276741). Briefly, genes with mean counts<10 were removed and CPM-normalized (counts per million) data was used to perform differential expression (DE) testing to identify GEP signatures. LS (least squares) mean values were calculated for each group as the linear combination or sum of the estimated means from the linear model. Due to the small sample sizes, we used Gene-Specific Analysis (GSA) to perform differential gene expression analysis between groups that applies a modified limma, an empirical Bayesian method, to detect the DE genes. Genes with LS > |1|, mean fold-change > |1| and $p < 0.05$ were considered as threshold for reporting significant differential gene expression [57]. Heatmaps were generated using unsupervised hierarchical clustering (HC) analysis based on the differentially expressed genes (DEGs).

2.16. Pathway analysis

Pathway analysis was performed to obtain insights into canonical biological pathways based on the differential expression of common gene sets. Ingenuity pathway analysis (IPA) software (QIAGEN) was used to identify the molecular pathways/mechanisms predicted to be activated or overexpressed, downregulated or co-regulated between the 3D models at Day 5 and Day 15, based on significantly differentially regulated gene set [58]. Further, Gene Set Enrichment Analysis (GSEA) was performed to interpret the gene expression data based on groups of genes that share common biological function, chromosomal location, or regulation [59]. GSEA generates a ranked list of genes from our expression dataset and then uses GSEAPreranked to analyze the ranked list and calculate normalized enrichment scores (NES), the primary statistic to interpret gene set/pathway enrichment/pathway results, based on ES for all dataset permutations [59].

2.17. Human RNAseq dataset

Finally, we compared our gene expression dataset on 3D samples (MS-Day15 and Agg-Day15) to bulk RNAseq data on healthy adult human heart samples obtained from previously published datasets (NCBI Bioproject accession number: PRJNA66731076).

2.18. Statistical analysis

Statistical analysis of the results was conducted using GraphPad Prism 9 (GraphPad Software, San Diego, CA), and the mean ± standard deviation (SD) was reported for all replicates. Outliers were identified and removed utilizing the robust regression and outlier removal (ROUT) method, with a coefficient Q value of 1 %. Subsequently, assessments were made to verify the assumptions of normal distribution and equality of variance. For data exhibiting a normal distribution (e.g., CM content on day 10, mitochondria area, sarcomere length, contraction frequency, and maximum contraction and relaxation velocities), a two-tailed, unpaired *t*-test was employed for the comparison of two groups. In contrast, non-normally distributed data (e.g., CM yield, changes in hiPSC-CM area over time in microsphere and aggregate, area and elongation and circularity between microsphere and aggregate, time interval contraction, and calcium propagation frequency and velocity), were analyzed using the Mann-Whitney test. In scenarios involving more than two groups and normal distribution (e.g., analysis of microsphere and aggregate phase contrast images for growth area, counting the total number of cells over time, and drug studies), a one-way analysis of variance (ANOVA) was conducted alongside Tukey's multiple comparison test. Alternatively, non-parametric ANOVA was applied for non-normally distributed data (e.g., calcium transient duration at 50 % and 80 %). A p-value of ≤0.05 was regarded as statistically significant. The following symbols and letters were used to denote statistical significance: "ns" indicated no statistical significance, * indicated $p \leq 0.05$; ** indicated $p \leq 0.01$; *** indicated $p \leq 0.001$; **** indicated $p \leq 0.0001$.

3. Results

3.1. Enhanced uniformity and reproducibility in scaffold-supported (microsphere) platform compared to the scaffold-free (aggregate) platform

We previously demonstrated the successful cardiac differentiation of hydrogel-encapsulated scaffold-supported (microsphere) hiPSCs, employing a microfluidic system to produce functional cardiac tissues [37]. Building upon this prior work, here we conducted an in-depth comparative analysis of cardiac tissues produced using this differentiation of hiPSCs within PF microspheres and those made using the 3D scaffold-free self-aggregation (aggregate) platform. The aggregate platform is the prevailing state-of-the-art approach to scale-up hiPSC-CM production in bioreactors [60]. We employed a cost-effective and chemically defined media for hiPSC expansion and differentiation in a suspension culture platform for microspheres and aggregates, which is amenable to scale-up hiPSC-CM production.

HiPSC-laden microspheres, produced via the microfluidic system at varying initial cell densities (30, 40, and 60 million hiPSCs mL^{-1}) (Supplementary Fig. 1), and aggregates formed through a shaker flask, were expanded, and differentiated under chemically defined media supplemented with CHIR on day 0, as depicted in Fig. 1A. The phase-contrast images after encapsulation indicated a uniform distribution of cells within a given batch (Fig. 1B). This microfluidic system has tight control over diameter (size) and axial ratio (shape), both within a batch and between batches for both tested hiPSC lines (Fig. 1C–E, Supplementary Fig. 1). In contrast, we observed more variability in size and shape within and between batches for aggregates compared to microspheres, particularly for Un-Arc 16 Facs II (Fig. 1C–E and Supplementary Fig. 1). This observation was drawn from fluorescent images of microspheres taken following microfluidic system formation (day −2) and phase-contrast images of aggregates taken immediately following the three-day shaker flask formation process (day 0) (Supplementary Fig. 1). The resulting microspheres exhibited an initial diameter of 673 ± 22 μm (coefficient of variation (CoV) = 3 %, n = 7 individual batches) and an axial ratio of 1.03 ± 0.01 (CoV = 1 %), whereas aggregates displayed an initial diameter of 166 ± 32 μm (CoV = 19 %, n = 7 individual batches) with an axial ratio of 1.137 ± 0.03 (CoV = 2 %). Viability assays conducted on day −2 (one day after encapsulation) for both hiPSC lines indicated that the majority of hiPSCs survived the encapsulation process, distributing uniformly throughout the PF hydrogel volume, as visualized by staining the nuclei (Fig. 1F and Supplementary Fig. 1). Likewise, robust viability of hiPSCs within the aggregates (day 0) was observed (Fig. 1G and Supplementary Fig. 1).

3.2. Cells maintained proliferative capacity and pluripotency in both platforms prior to initiation of cardiac differentiation

Cell morphology, proliferation, pluripotency, and Collagen I deposition were visualized through immunostaining of microspheres using phalloidin (which stains actin filaments, also known as F-actin), Ki67, Oct4, and Collagen I (as shown in Fig. 2 and Supplementary Fig. 2). HiPSCs maintained their formation of rounded colonies throughout whole microspheres. Both the microsphere and aggregate platforms exhibited positive expression of proliferation and pluripotency markers prior to cardiac differentiation (day 0). Prior to initiation of cardiac differentiation, Collagen I deposition was observed only in the aggregate platform. Therefore, both platforms could successfully support stem

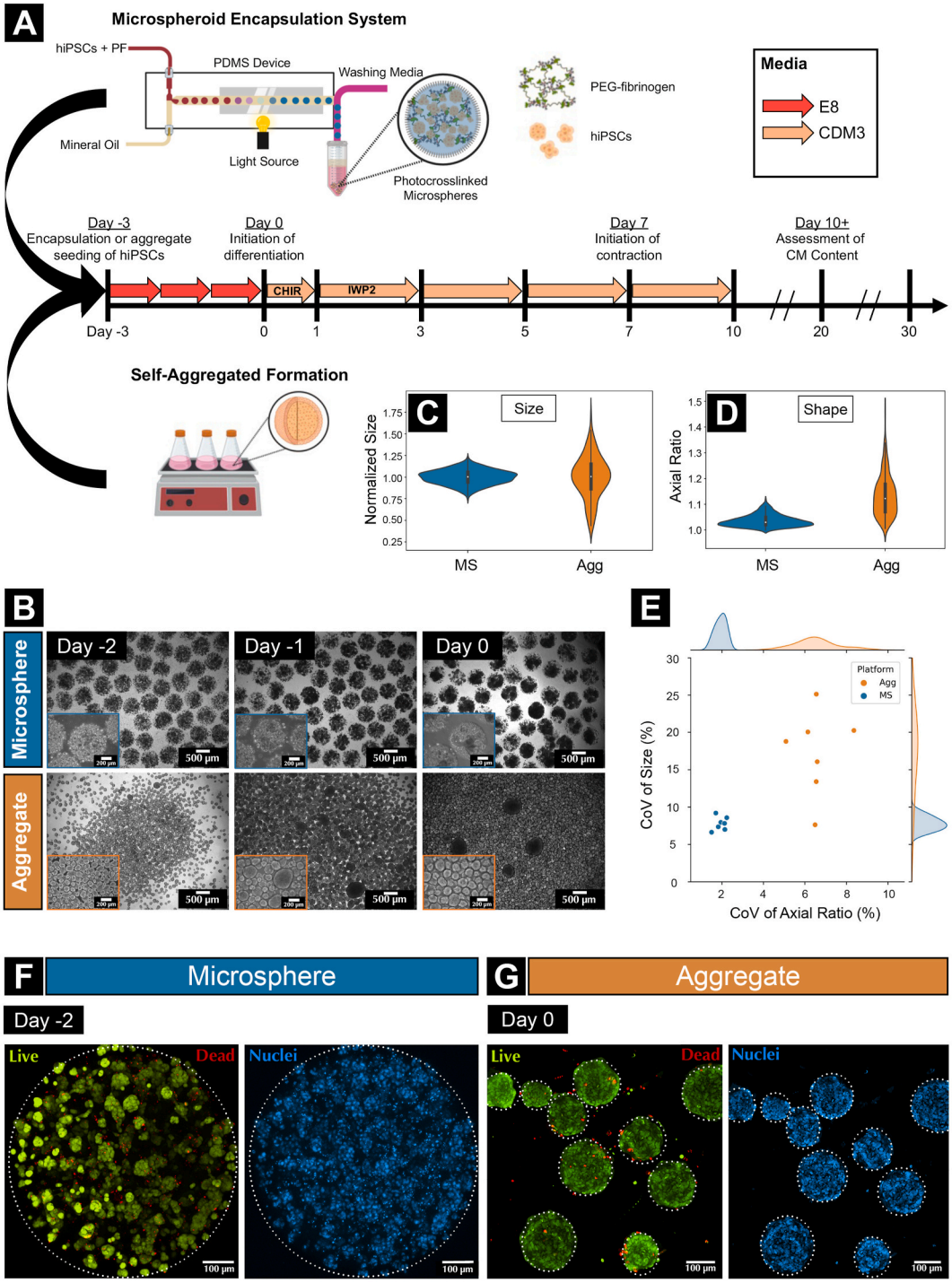

Fig. 1. Application of scaffold-supported (microsphere) and scaffold-free (aggregate) approaches for 3D hiPSC tissue production under chemically defined conditions (A) Schematic of microsphere production through hiPSC encapsulation within PF hydrogels and aggregate formation through seeding a single-cell suspension in a shaker flask on day −3. Cardiac differentiation was initiated by activating Wnt on day 0, followed by inhibition on day 1. Media exchange with fresh CDM3 occurred on days 3, 5, and 7. (B) Phase contrast images throughout the time course before starting differentiation visually showed an increase in cell numbers within the hydrogels as well as cell growth in the aggregate platform. (C, D) The microfluidic system tightly controlled microsphere diameter (size) and axial ratio (AR, shape), enabling the generation of highly uniform microspheres within and between batches (n = 7 batches, comprising at least 30 microspheres and aggregates analyzed per batch). (E) Coefficient of Variation (CoV) for size and shape within each batch of microspheres and aggregates depicted in a joint plot, indicating that the encapsulation platform produced microspheres with greater uniformity between batches compared to self-aggregate formation. (F, G) Post-encapsulation and -aggregate seeding, hiPSCs maintained substantial cell viability.

cells in maintaining their proliferative and pluripotency phenotype before initiating differentiation.

3.3. Microsphere encapsulation enhanced uniformity between batches and increased cell production

After the initiation of cardiac differentiation (day 0), cells in both

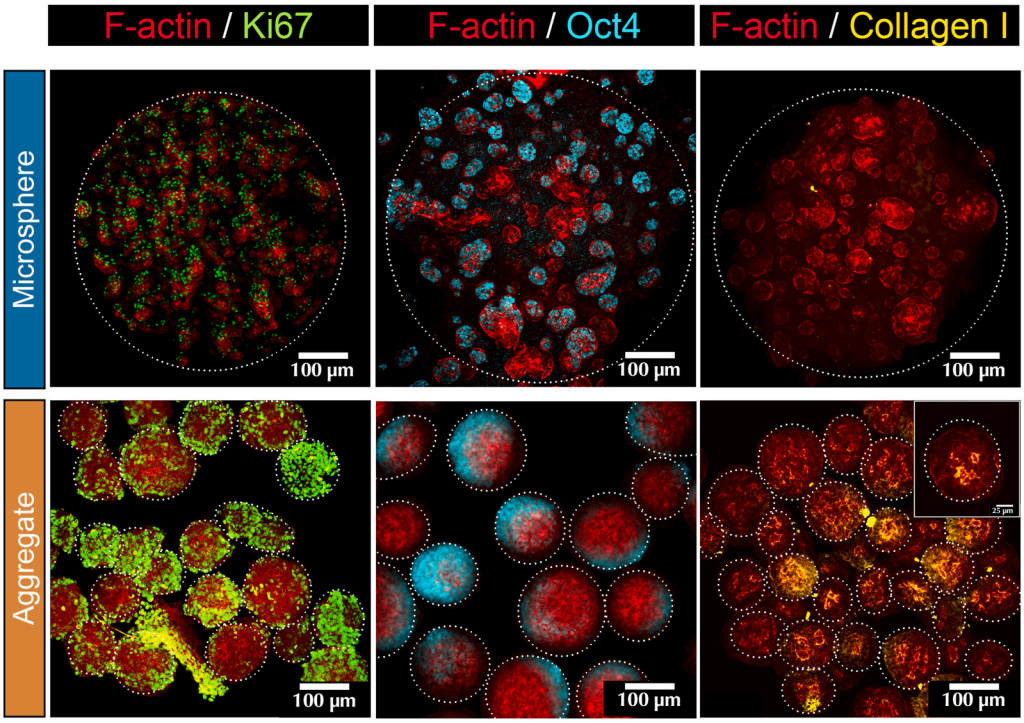

Fig. 2. Maintenance of proliferative capacity and pluripotency in HiPSCs within microspheres and aggregates. Confocal immunofluorescence images depict Phalloidin staining (in red) to visualize F-actin filaments, the proliferation marker Ki67 (in green), the pluripotency marker Oct4 (in cyan), and collagen I (in yellow) for extracellular matrix (ECM) production on day 0 before initiating differentiation.

platforms began to grow, forming continuous tissues as depicted in Fig. 3A and Supplementary Fig. 3A. The normalized growth area of microspheres and aggregates from day 0 exhibited higher variation between batches in the aggregate platform than in microspheres, especially on days 1 and 3 (n = 4 individual batches, shown in Fig. 3B, C and Supplementary Figs. 3B and C). For the Un-Arc 16 Facs II hiPSC line, the normalized growth area of microspheres remained consistent until day 3 and increased significantly by 68 % on day 5 compared to day 0. On the other hand, the normalized growth area of aggregates exhibited a significant 85 % increase on day 3 compared to day 0. The IMR90 cell line followed a similar trend in both platforms, but the percentage change was lower (Supplementary Figs. 3B and C). Cell counts were taken on days 0, 5, and 10, and these counts were normalized to the counts on day −3 for both platforms (n = 5 individual batches for microspheres and 4 for aggregates, illustrated in Fig. 3D and E and Supplementary Figs. 3D and E). The results for the Un-Arc 16 Facs II cell line demonstrated a significant 59 % increase in the total number of cells within the microsphere platform on day 10 compared to day −3 and a 28 % increase for the IMR90 cell line. In contrast, the aggregate platform experienced a notable 45 % decrease in the total cell count on day 10 as compared to day 0 for both hiPSC lines. These results indicate that the microsphere platform provides a significantly higher total number of cells per initial hiPSC.

3.4. Enhanced cardiac differentiation efficiency and mature-like mitochondrial organization observed in hiPSC-CMs from the microsphere platform

Encapsulation of hiPSCs within the hydrogel matrix prior to initiating differentiation had a notable impact on both cardiac differentiation outcomes and the contraction functionality of the resulting cardiac tissues. For both Un-Arc 16 Facs II and IMR90 lines, the microspheres had a higher percentage of CMs on day 10 in comparison to aggregates. Differentiation of microsphere-encapsulated hiPSCs resulted in 68.4 ± 17.7 % and 71.9 ± 5.5 % CMs, respectively, while the aggregate CM content was 53.8 ± 23.6 % and 33.1 ± 7 % based on flow cytometry data (Fig. 4A and Supplementary Fig. 4F). These results are from cTnT+ and MF20+ populations, with data collected from n = 35 batches for microspheres and 19 batches for aggregates for the Un-Arc 16 Facs II line, and n = 2 batches for microspheres and 3 batches for aggregates for the IMR90 line ($p < 0.05$) without the application of any purification method such as glucose starvation. Additionally, microspheres had a significantly higher number of CMs per initial hiPSC (2.1 ± 1.8 for Un-Arc 16 Facs II and 0.9 ± 0.02 for IMR90) than aggregates (0.6 ± 0.5 for Un-Arc 16 Facs II and 0.19 ± 0.07 for IMR90) on day 10 (n = 21 and 19 individual batches for Un-Arc 16 Facs II and n = 2 and 3 individual batches IMR90, respectively, $p < 0.05$) (Fig. 4B and Supplementary Fig. 4G). The initial hiPSC density in PF did not significantly affect the cardiac differentiation outcome (Supplementary Figs. 3A–C). Three platforms were used for aggregate seeding and differentiation: shaker flask ('F'), well plate ('P'), and a hybrid approach involving seeding in a shaker flask until day 0, followed by differentiation in a well plate ('F/P'). Across the three different platforms for aggregate seeding and differentiation (F, P, F/P), no significant differences were noted in terms of CM content and CM yield (Supplementary Figs. 3D and E).

To apply a validated, unbiased monolayer cell segmentation algorithm that operates independently of user input, we replated the hiPSC-CMs from day 20 and 30 dissociated microspheres and aggregates on a Matrigel-coated glass surface. This approach allowed for the automatic segmentation of individual cells and the extraction of detailed morphological data. Staining was performed for sarcomere, connexin 43 (Cx43), mitochondria, and nuclei. Representative images for day 30 are depicted in Fig. 4C. Cx43 was observed at the junction sites, and mitochondria were evenly distributed throughout the hiPSC-CMs derived from the microsphere platform. Conversely, in the case of aggregates, mitochondria were predominantly located near the nuclei. The mitochondria area of hiPSC-CMs from microspheres and aggregate platforms on day 30 were 2.1 ± 0.5 μm^2 and 1.4 ± 0.4 μm^2, respectively (Fig. 4D, $p < 0.0001$, n ≥ 19 cells for each group). To assess cell morphology, we adopted an unbiased algorithm [52], for automatic segmentation and

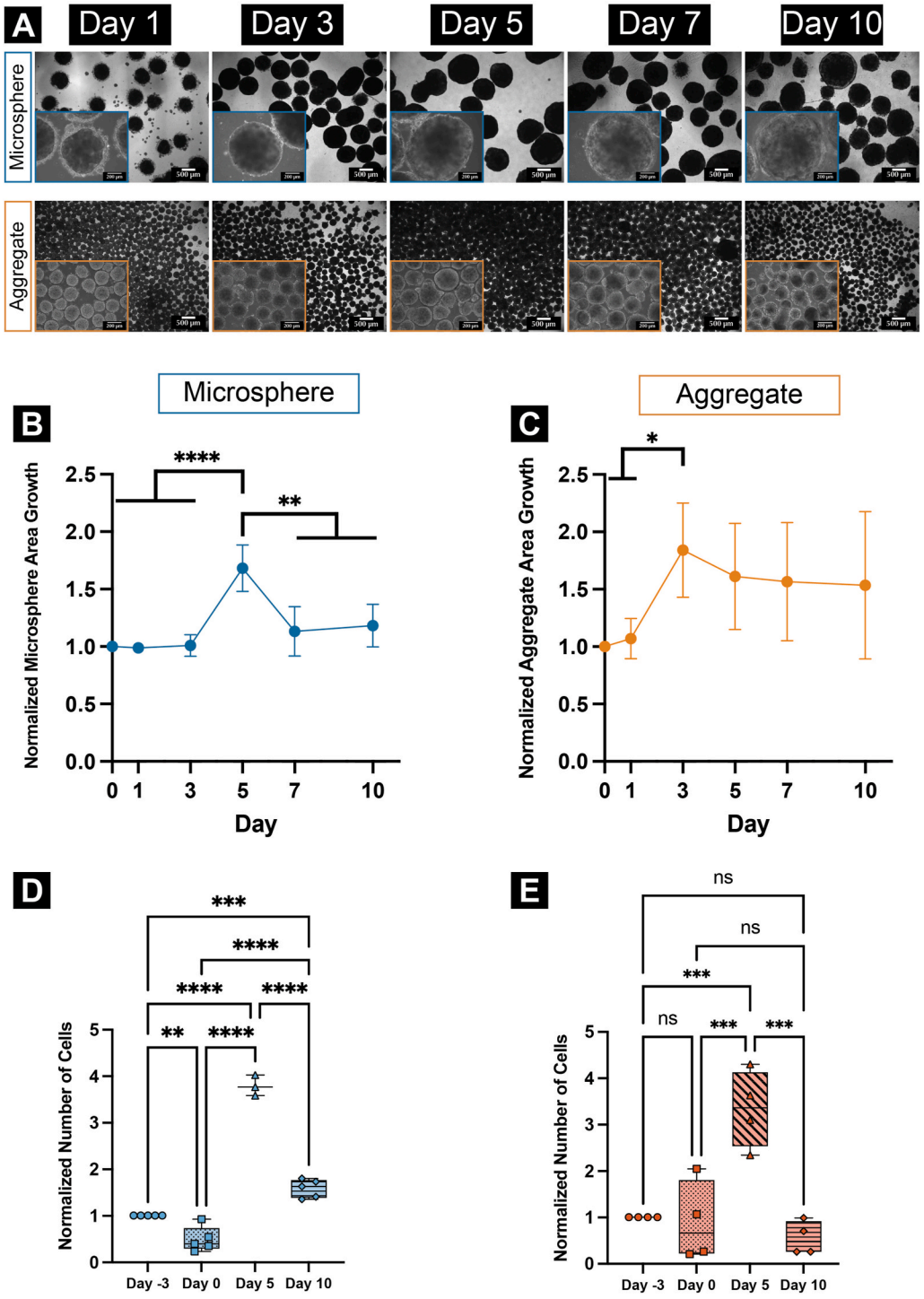

Fig. 3. Continued growth of encapsulated cells and aggregates over time during differentiation, with microspheres exhibiting a significantly higher normalized cell count at day 10. (A) Phase-contrast images of microspheres and aggregates throughout differentiation visually illustrated the progression of differentiating cells in PF microspheres and revealed an increasing cell density within the aggregates up to day 5. (B) Normalized microsphere growth area remained consistent until day 3 and then significantly increases by 68 % on day 5 compared to day 0. (C) Normalized aggregate area significantly increased by 85 % between days 3 and 0 (*$p < 0.05$, $n = 4$ individual batches). (D) The total number of cells in the microspheres platform significantly increased by 59 % on day 10 compared to day −3 (**$p < 0.01$, ****$p < 0.0001$, $n = 5$ individual batches). (E) The total number of cells in the aggregate platform decreased significantly by 45 % on day 10. (***$p < 0.001$, ****$p < 0.0001$, $n = 5$ different batches).

texture analysis (Supplementary Fig. 4H and I) and for sarcomere length measurement, we employed a second MATLAB algorithm, SarcTrack, developed by Toepfer et al. [53]. For hiPSC-CMs from the microsphere platform, a significant increase in cell area was observed over time (from 1921 ± 1182 μm^2 on day 20 to 3397 ± 2246 μm^2 on day 30, Fig. 4E, $p<0.0001$, $n \geq 55$ cells), consistent with reports of CM size increases during heart development [61]. For hiPSC-CMs from the aggregate platform, a significant increase in cell area over time was not observed; aggregate hiPSC-CM cell area was 1704 ± 940 μm^2 on day 20 and 1879 ± 1443 μm^2 on day 30 (Fig. 4E). In addition, hiPSC-CMs from

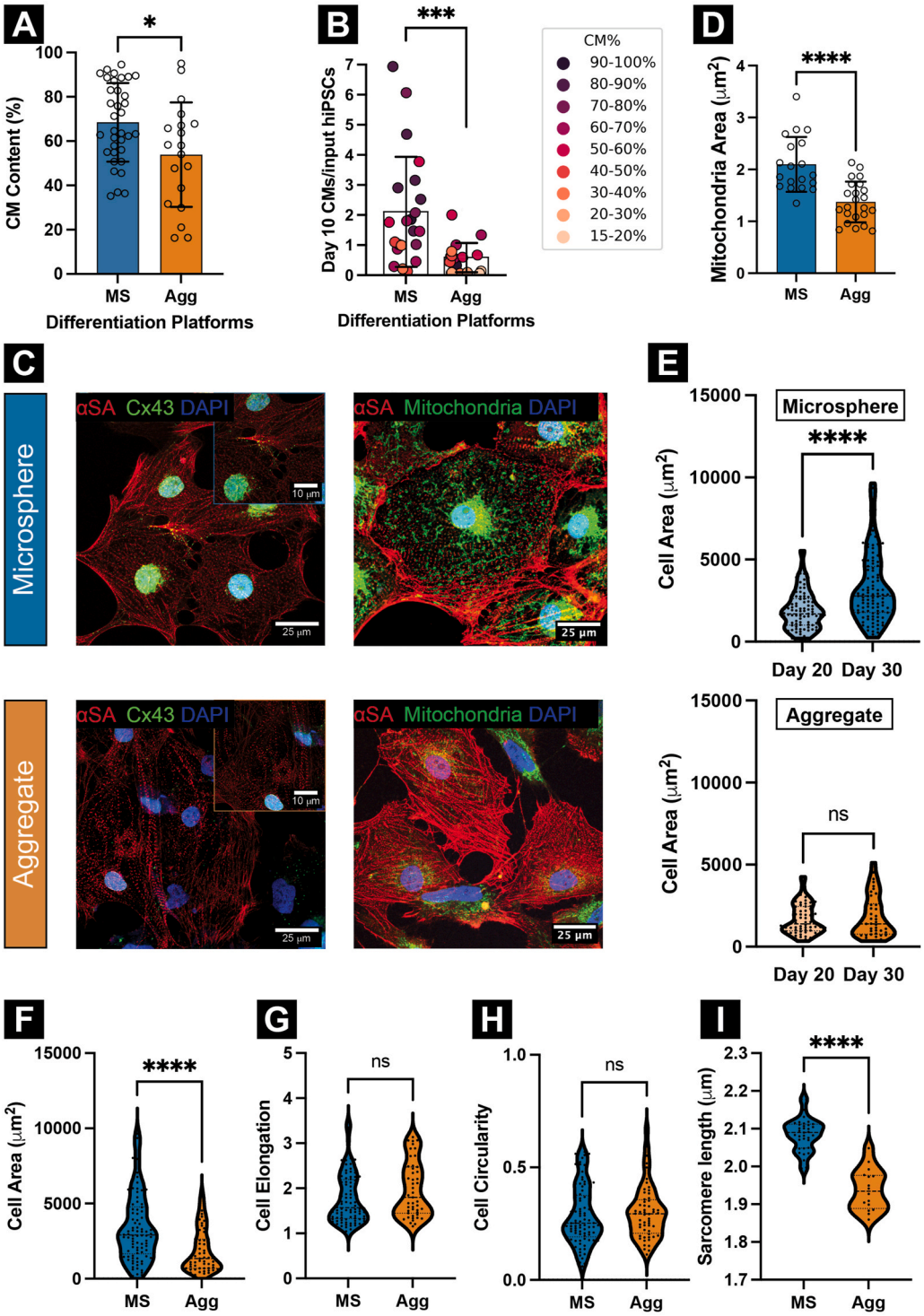

Fig. 4. Higher cardiac content and yield occurred in the microsphere platform compared to the aggregate platform with more structural mature-like mitochondria organization in resulting hiPSC-CMs. (A) Microsphere and aggregate platforms contained 68.4 ± 17.7 % and 53.8 ± 23.6 % CMs (cTnT+) on day 10, respectively (*$p < 0.05$, for microsphere n = 35 individual batches and for aggregate n = 19 individual batches). (B) The cardiomyocyte yield, represented by the ratio of the number of CMs on day 10 over the initial number of stem cells on day −3, was 2.1 ± 1.8 for microspheres and 0.6 ± 0.5 for aggregates (***$p < 0.001$, n = 22 individual batches for microsphere, n = 19 individual batches for aggregate). (C) Immunostaining of dissociated hiPSC-CMs in the microsphere and aggregate platforms on day 30 (αSA, red; Nuclei, blue; Cx43, green in left images, Mitochondria, green in right images). (D) The mitochondria area of hiPSC-CMs from microspheres and aggregate platforms on day 30 were 2.1 ± 0.5 μm^2 and 1.4 ± 0.4 μm^2, respectively (****$p < 0.0001$, n ≥ 19 cells for each group). (E) Cell area of hiPSC-CMs from microspheres increased significantly over time, while that of hiPSC-CMs from the aggregate platform remained unchanged. (F) Average cell area of hiPSC-CMs from the microsphere and aggregate platforms on day 30 were 3397 ± 2246 and 1879 ± 1443 μm^2, respectively. (G) Cell elongation of hiPSC-CMs from microsphere and aggregate platform were 1.78 ± 0.55 and 1.97 ± 0.6, respectively. (H) Cell circularity of hiPSC-CM from microsphere and aggregate platform were 0.28 ± 0.13 and 0.3 ± 0.11, respectively. (I) The sarcomere length of hiPSC-CMs from the microsphere and the aggregate platforms were 2.08 ± 0.04 and 1.94 ± 0.05 μm, respectively (for E-I: ****$p < 0.0001$, n ≥ 55 cells were included, comprising data from four individual batches of microspheres and two individual batches of aggregates).

microspheres had a significantly higher cell area than hiPSC-CMs from aggregates on day 30 (Fig. 4F, $p<0.0001$, $n \geq 55$ cells for each group from 4 individual batches for the microsphere platform and 2 individual batches for the aggregate platform). The other morphological properties, such as cell elongation and circularity were statistically the same for hiPSC-CMs from both platforms (Fig. 4G and H). The average sarcomere length of hiPSC-CMs from the microsphere platform (2.08 ± 0.04 μm) was significantly tgreater than that of hiPSC-CMs from the aggregate platform (1.94 ± 0.05 μm) (Fig. 4I, $p<0.0001$, $n \geq 55$ cells). Furthermore, to visualize the cellular organization within the microspheres and aggregates, immunostaining of intact tissues for cTnT and Collagen I was performed on day 37 of differentiation. The results are presented in Supplementary Figs. 4J and 4K, as well as in Supplementary Movies 5 and 6.

3.5. Microspheres on day 10 contracted faster than aggregates and their contraction velocity continued to increase over time

Myocardial contractility was enhanced in cardiac microspheres compared to aggregates (with similar average CM content on day 10, Fig. 5, Supplementary Movies 1-4). The maximum contraction velocity for microspheres was four times higher than that of aggregates (141.8 ± 12.5 μm/s versus 36.2 ± 6 μm/s), while the maximum relaxation velocity was nine times higher (97 ± 7.2 μm/s versus 10.8 ± 5.8 μm/s) (Fig. 5A–D, $p<0.001$, $n = 3$ independent batches for each platform). Furthermore, microspheres exhibited faster contraction (a 77 % increase) and relaxation (a 113 % increase) velocities over time (Fig. 5E, $p<0.05$, $n = 3$ independent batches). Conversely, no significant differences in the contractile functionality of aggregates were observed with

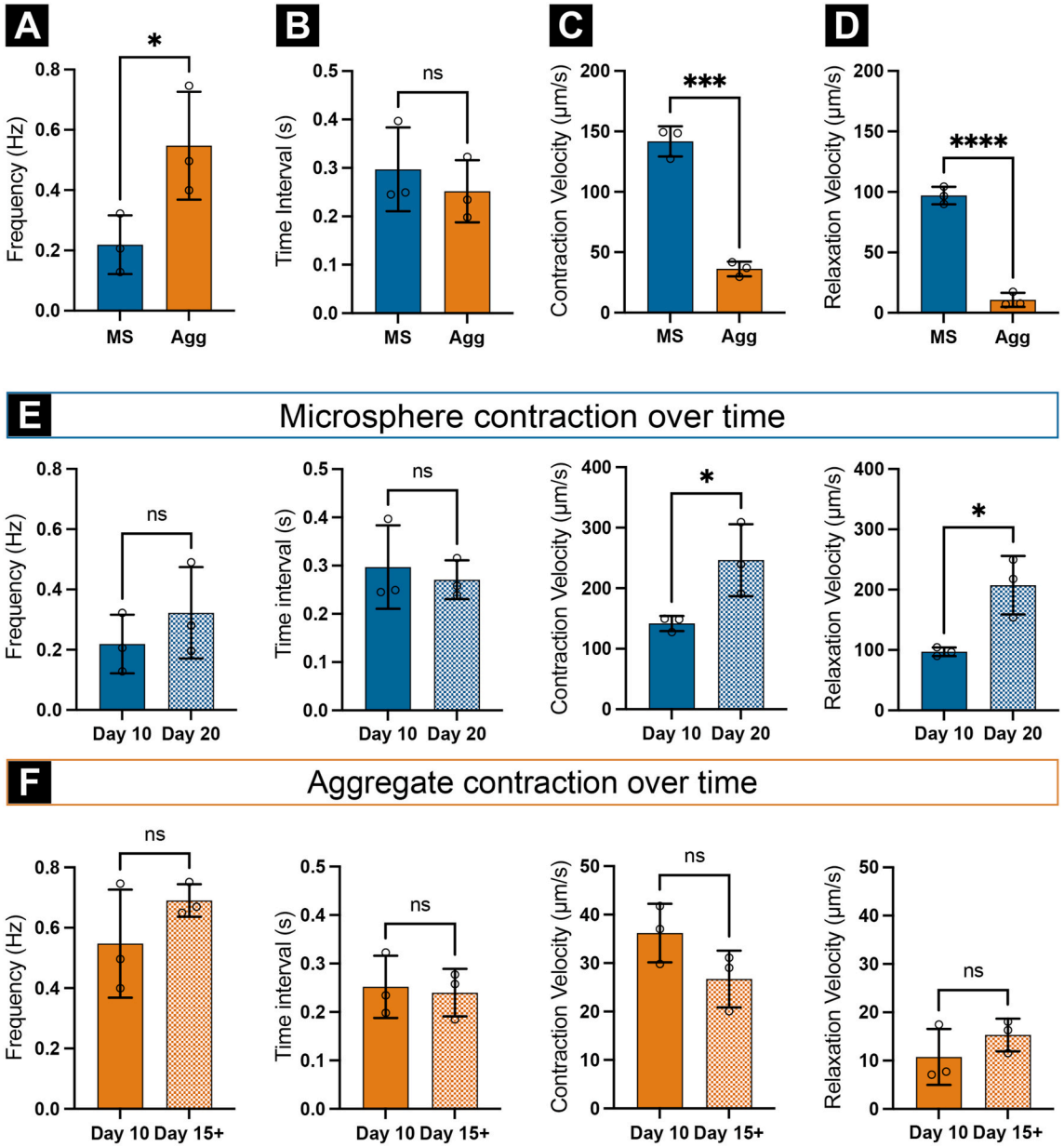

Fig. 5. Microspheres exhibited enhanced contractile functionality and evolved into a tissue with faster contraction during extended periods of culture. (A) The contraction frequencies for microspheres and aggregates were 0.22 ± 0.079 and 0.55 ± 0.18 Hz, respectively. (B) Time interval, representing the duration between contraction and relaxation, was 0.3 ± 0.08 ms for microspheres and 0.25 ± 0.06 ms for aggregates. (C and D) On day 10, the contraction and relaxation velocities for the microsphere platform were 141.8 ± 12.5 μm/s and 97 ± 7.2 μm/s, respectively, while those for the aggregate platform were 36.2 ± 6 μm/s and 10.8 ± 5.8 μm/s. (E) Microspheres showed faster contraction (77 % increase) and relaxation (113 % increase) velocities over time. (F) No significant improvements in the contractile functionality of aggregates were observed during extended culturing periods (*$p < 0.05$, ***$p < 0.001$, ****$p < 0.0001$, $n = 3$ batches).

extended time of culturing (Fig. 5F).

Similar results were observed for the IMR90 cell line; contraction analysis on day 10 revealed significantly faster contraction (five times higher) and relaxation (nine times higher) velocities in microspheres compared to aggregates ($n \geq 10$ tissues from two individual batches, $p < 0.0001$) (Supplementary Figs. 5C and D). The magnitude of these velocities, as well as the improvement in contraction and relaxation, was consistent between the two hiPSC lines.

3.6. Microsphere hiPSCs-CMs β-adrenergic signaling may be more mature than aggregates and showed appropriate electrophysiological properties

Furthermore, the capacity of hiPSC-CMs to appropriately respond to β-adrenergic agonist (isoproterenol- Iso) and antagonist (propranolol-Pro) pharmacological stimulation was compared. Microspheres significantly responded (frequency increased 124 % (Iso) and decreased 61 % (Pro)), whereas for aggregates, changes in contraction frequency were less pronounced (frequency increased 49 % (Iso) and decreased 27 % (Pro)) (Fig. 6A–D). These results suggest that microsphere hiPSC-CM β-adrenergic signaling may be more mature.

The electrophysiology of cardiac tissues from microspheres and aggregates was evaluated by optical mapping of calcium transient propagation. Microsphere spontaneous depolarization rates were 0.32 ± 0.03 Hz; aggregate spontaneous depolarization rates were 0.55 ± 0.07 Hz. During spontaneous depolarization, calcium transient durations at 50 % (CTD50) and 80 % (CTD80) repolarization were 554 ± 8.42 ms and 1075 ± 34.88 ms, respectively, for microspheres and 418 ± 25.13 ms and 890 ± 70.8 ms, respectively, for aggregates. Calcium transient velocity was 0.62 ± 0.24 and 0.58 ± 0.14 cm/s for microspheres and aggregates, respectively (Fig. 6F–H, n = 3 recordings). Calcium transient propagation was more uniform in microsphere-differentiated hiPSC-CMs than aggregate differentiated hiPSC-CMs; no significant differences were observed in CTD or calcium transient velocity.

3.7. Comparative transcriptome analysis revealed enhanced cardiomyocyte differentiation and contractile functionality in microsphere platform

To evaluate the impact of stem cell encapsulation on transcriptomic changes during and after differentiation, we compared the temporal changes within each platform as well as the differences between platforms at specific time points (GEO: GSE276741). At a significance threshold of $p < 0.05$, next-generation mRNA sequencing analysis revealed that 4139 genes were differentially expressed between the MS-Day 15 vs MS-Day 5 (fold-difference≠1). Among these, 2016 genes had a fold change difference of >2 or < -2 (>|2|). Within the total of 4814 genes that were differentially expressed between the Agg-Day 15 vs Agg-Day 5 (fold-difference≠1), 2576 had a fold change difference of >|2|.

Comparing the differentially expressed genes (DEGs) across time (day 15 vs. day 5) in each platform, over 60 % of the DEGs, or 2855 genes, were common between the two platforms, along with a comparable number of up- and down-regulated genes (Fig. 7A). Additionally, it was demonstrated that 1960 genes were exclusive to the aggregate platform, while 1284 genes had distinct differential expression in the microsphere platform across time ($p < 0.05$). These results suggest that the systems have both common and distinct regulating mechanisms.

The genes that were associated with cardiomyocyte differentiation (GO:0055007), heart development (GO:0007507), cardiac muscle contraction (GO:0060048), and sarcomere organization (GO:0045214) were plotted for microsphere day 15 vs. day 5 and aggregate day 15 vs. day 5 (Fig. 7B). The temporal pattern of gene expression was similar for both the microsphere and aggregate platforms, with most genes showing upregulation on day 15 versus day 5. However, the microsphere platform exhibited a higher magnitude of upregulation, and a lower degree of downregulation compared to the aggregate platform over time. This suggests that the microsphere platform may provide a more conducive environment for the differentiation and maturation of cardiomyocytes.

Violin plots of $\log_2$ fold changes within the top gene ontologies (GO) on days 5 and 15 revealed that the microsphere platform had a greater degree of gene expression across various biological processes crucial to heart function (Fig. 7C and D, Supplementary Table 2). Red represents a positive fold change, indicating increased expression in microspheres. Conversely, blue represents a negative fold change, indicating higher expression in aggregates. The width of the violin plot is proportional to the gene density within each gene ontology region. The majority of the genes in the cell adhesion gene ontology exhibited a positive fold change (higher on the microsphere platform) on both days 5 and 15. This observation suggests that the presence of biomaterial might potentially enhance cell-cell adhesion in the microsphere platform. Furthermore, many of the genes involved in the control of heart contraction and cardiac muscle contraction exhibited a positive fold change (indicating increased expression in the microsphere platform) on day 15, which is consistent with the observed contractile functionality findings.

This enhanced gene expression profile was corroborated by volcano plot analyses, which showed a broader range of significantly regulated genes in the microsphere platform compared to the aggregate platform on both time points (Fig. 7E and F and Supplementary Fig. 6). Notably, the expression of H19 differed between day 5 and day 15 in both the microsphere and aggregate platforms. On day 5, the microsphere platform showed a greater level of expression of H19 compared to the aggregate. On day 15, the microsphere platform exhibited significantly reduced expression of H19 compared to the aggregate, with a high level of statistical significance. This indicates that H19 suppresses the levels of let-7 micro-RNAs69, which are responsible for promoting cardiac maturation [62]. Also, cardiomyocyte structural genes such as TTN (the sarcomere-spanning protein titin) and MYOM1 (Myomesin-1) showed significantly higher expression in the microsphere platform compared to the aggregate platform.

Pathway analysis of the differentially expressed gene sets revealed a consistent trend in activation and inhibition between the microsphere and aggregate conditions on day 15 (Fig. 7G). Nevertheless, there was a discrepancy in the extent of activation and inhibition seen on the two platforms. For pathways related to cell structure (actin cytoskeleton signaling, cardiac hypertrophy signaling, striated muscle contraction), cell adhesion (integrin-linked kinase (ILK) signaling), and functionality (cardiac conduction, calcium signaling, protein kinase A signaling), the microsphere platform showed increased activation levels. These results are consistent with the reported characteristics of cell morphology and contractility, as shown in Figs. 4 and 5. The Gene Set Enrichment Analysis (GSEA) plot revealed a substantial enrichment and upregulation of the Wnt signaling pathway in the microsphere platform compared to the aggregate platform on both day 5 and day 15 (Fig. 7H). Therefore, it may be inferred that the microsphere platform may result in increased activation of the Wnt signaling pathway. Furthermore, the pathway responsible for the development of striated muscle tissue showed a considerable enrichment and increased activity in microsphere-engineered cardiac tissues compared to aggregates on day 15. Although there was some enrichment and overexpression in the striated muscle contraction pathway on day 15 in the microsphere condition, it was not as substantial as in other pathways, such as striated muscle tissue formation or Wnt signaling.

To assess the variation between ECTs generated using the microsphere and aggregate platforms and adult cardiac tissue, the transcriptome of adult cardiac tissue (PRJNA66731076) was compared with the transcriptome of ECTs formed using the microsphere and aggregate platforms on day 15 (Fig. 7I). The results indicated that both microsphere and aggregate tissues show a similar level of difference from adult tissue, following the same pattern. However, when it comes to sarcomere-associated processes, oxidative phosphorylation, and fatty acid transport, the average $\log_2$ fold change was somewhat closer to the baseline. To get a more comprehensive comparison, it would be more informative to examine subsequent time intervals of both microsphere

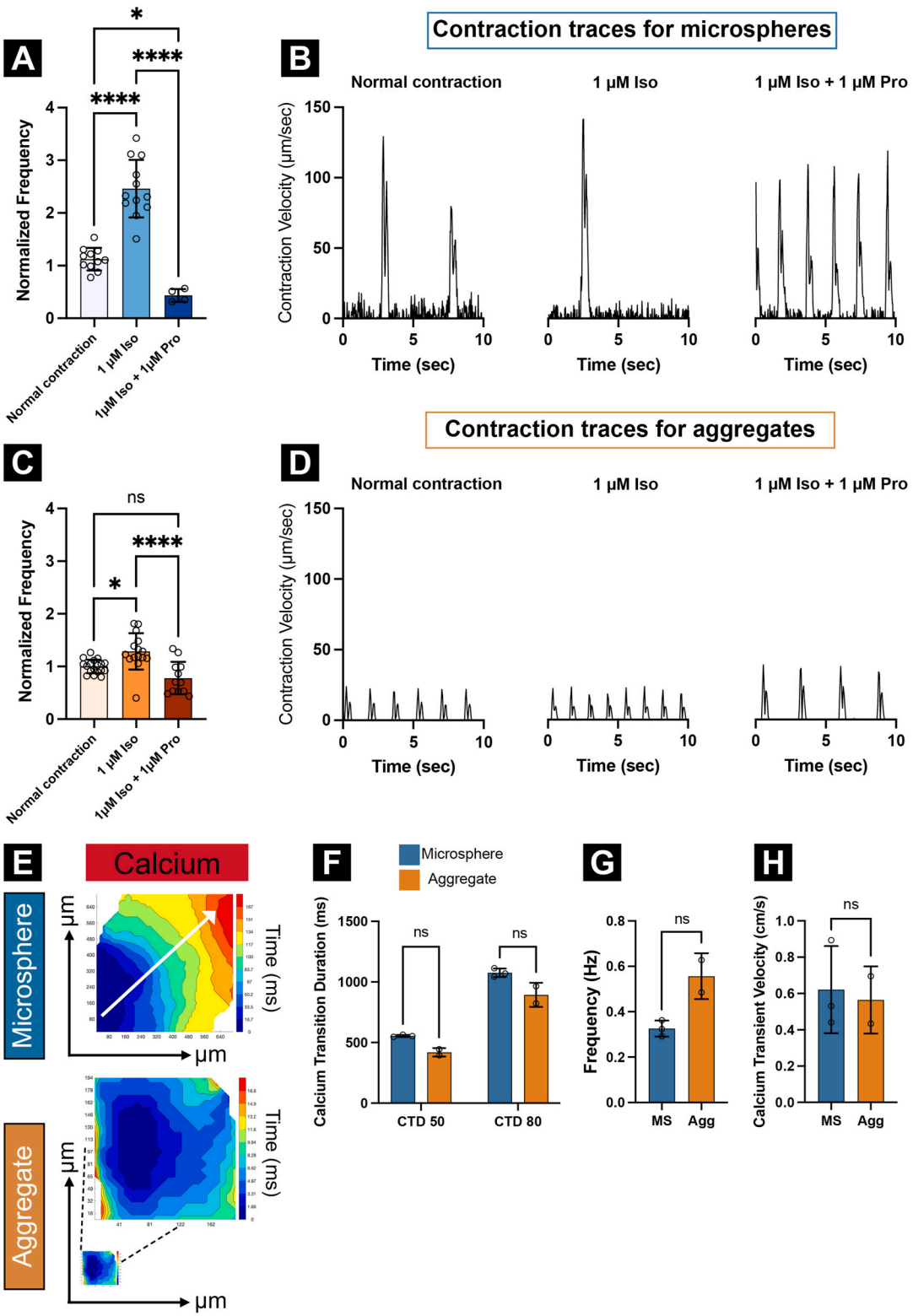

Fig. 6. Microspheres and aggregates responded appropriately to pharmacological stimulation. (A) Responses to β-adrenergic agonist (isoproterenol- Iso) and antagonist (propranolol- Pro) as pharmacological stimulation of microspheres. Microsphere contraction frequency increased 124 % (Iso) and decreased 61 % (Pro) with respect to normalized contraction frequency. (B) Representative analyzed traces for microspheres after incubating in Iso and Pro as indicated. (C) Changes in contraction frequency of aggregates were less pronounced (frequency increased 49 % (Iso) and decreased 27 % (Pro). (D) Representative analyzed traces for aggregates after incubating in Iso and Pro as mentioned. (*$p < 0.05$, ****$p < 0.0001$, $n \geq 4$ microspheres from 2 individual batches and $n \geq 12$ aggregates from 3 individual batches.) (E) Calcium transient propagation in microspheres and aggregates was evaluated by optical mapping (day 20). Microspheres showed uniform calcium transient propagation. (F) Calcium transient durations (CTDs) at 50 % and 80 % repolarization were 554 ± 8.42 and 1075 ± 34.88 ms for microspheres and 418 ± 25.13 and 890 ± 70.8 ms for aggregates, respectively (n = 3 recordings). (G) The frequency of spontaneous calcium transient propagation was 0.32 ± 0.03 and 0.55 ± 0.07 Hz for microspheres and aggregates, respectively (n = 3 recordings). (H) Calcium transient velocity was 0.62 ± 0.24 and 0.58 ± 0.14 cm/s for microspheres and aggregates, respectively (n = 3 recordings).

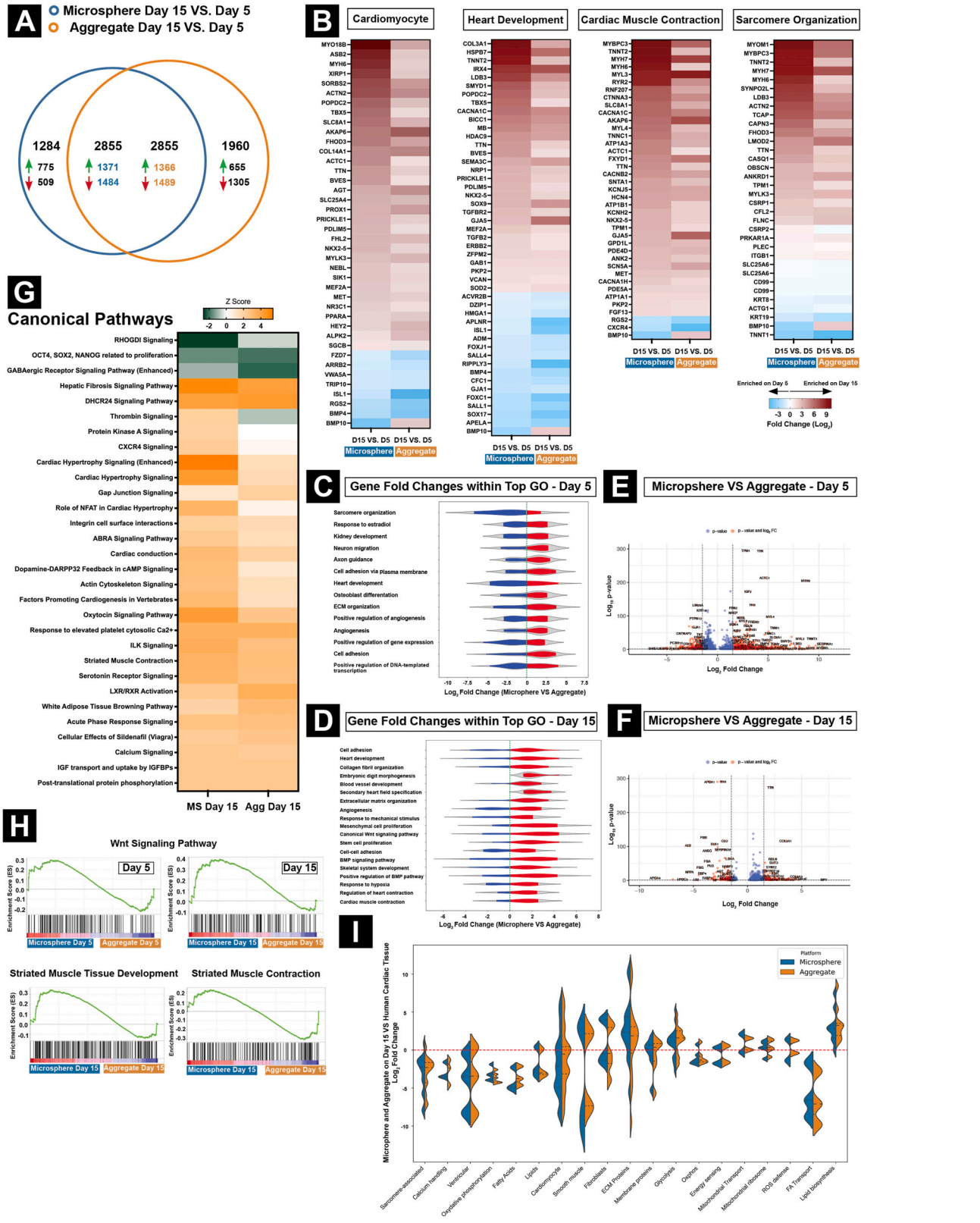

(caption on next page)

Fig. 7. Microsphere and aggregate platforms show similar transcriptome trends but higher gene expression levels in microspheres. (A) Differentially expressed genes (DEGs) temporal comparison between microsphere (from day 15 to day 5) and aggregate (from day 15 to day 5) platforms revealed 2855 common genes with similar numbers of up- and down-regulated genes. Additionally, 1284 genes were differentially expressed only in the microsphere platform and 1960 genes were differentially expressed only in the aggregate platform. (B) Heatmap representing genes associated with cardiomyocyte differentiation, heart development, cardiac muscle contraction, and sarcomere organization for microsphere day 15 vs. day 5 and aggregate day 15 vs. day 5. The direction of gene regulation (up or down) from day 5 to day 15 is the same between microsphere and aggregate platforms, but microsphere platform exhibits more pronounced transcriptional changes compared to the aggregate platform. (C, D) Violin plot of the $\log_2$ fold change between microsphere and aggregate on days 5 and 15 for top gene ontologies (p-value $\leq$0.05, fold enrichment $\geq$2, gene count $\geq$10), respectively (E, F) Volcano plot comparing microsphere vs. aggregate on days 5 and 15, respectively. Red points represent genes with significant p-values and $\log_2$ fold change, while blue points represent genes with significant p-values only. (G) Canonical pathway analysis for microsphere and aggregate on day 15. (H) Gene Set Enrichment Analysis (GSEA) plot for Wnt signaling pathway (both days 5 and 15), striated muscle tissue development, and striated muscle contraction for microsphere vs. aggregate on day 15. (I) Comparison of microsphere and aggregate on day 15 vs. adult human cardiac tissue (PRJNA66731076).

and aggregate tissues.

4. Discussion

In this study, we differentiated hiPSCs into CMs using both scaffold-supported (microsphere) and scaffold-free (aggregate) platforms under chemically defined, scalable conditions. The PEG-fibrinogen (PF) hydrogel, chosen for its clinical relevance [63], created a 3D microenvironment conducive to both hiPSC expansion and CM differentiation. Our previous studies using both microfluidic [37] and mold-based [38,40,64] approaches to form the hiPSC-laden engineered tissues have demonstrated the successful cardiac differentiation of hydrogel-encapsulated hiPSCs. These studies underscore that this approach can promote a high degree of CM maturation, including T-tubule formation [64], and appropriate responses to external pacing [40], in static culture conditions. To assess whether our approach could address challenges inherent in existing aggregate differentiation and offer a more scalable and clinically applicable system, we investigated the relative characteristics of hiPSC-laden hydrogel microspheres and hiPSC aggregates in chemically-defined, suspension-based, differentiation conditions. Our work provides the first direct comparison of hiPSC-laden hydrogel microspheres and aggregates in suspension-based differentiation, highlighting the microsphere platform's superior performance in enhancing cell production and structural maturation of hiPSC-CMs. Furthermore, the microsphere platform improves contractile functionality, responses to pharmacological stimulation, and more uniform calcium transient propagation in resulting cardiac tissues.

Encapsulation of both hiPSC lines in biomimetic PF hydrogels offered tighter control over the cellular microenvironment, enhancing batch-to-batch consistency with high post-encapsulation cell viability, as shown in Fig. 1. The consistent size and shape uniformity observed within batches (Supplementary Fig. 1), along with the reproducibility of microspheres (Fig. 1E), are of paramount importance for various biomedical applications, including high-throughput screening, cell production, and cell therapy. Unlike the aggregate platform, which exhibited significant size variability (Fig. 1C–E), consistent with earlier aggregate suspension-based studies [65,66], the microsphere approach demonstrated superior reproducibility (Fig. 1E). To improve differentiation consistency in a suspension-based aggregate formation system, Kahn-Krell et al. filtered out large aggregates [67]; the potential downside of this approach is the application of additional shear stress to the cells/aggregates prior to starting differentiation. Previous studies have attempted to control aggregate size during initial generation and long-term culturing, as reviewed by Sart et al. [68]. Some strategies, including the utilization of V-shaped well plates [69,70] for cell seeding and aggregate formation to attain uniform size and shape, encountered challenges when applied to scale-up studies. In another study, embryonic stem cells (ESCs) have been encapsulated in alginate microcapsules with a liquefied core for cardiac differentiation [41]. In this approach, the ESC aggregate size within the alginate was adjusted by controlling the concentration of seeded ESCs. In contrast to other cell encapsulation systems that use lower cell densities and require longer crosslinking times as previously compared [42], the microsphere platform demonstrates scalability by efficiently encapsulating an average of one million stem cells per minute.

Suspension-based differentiation platforms have enabled scalable hiPSC-CM production via scaffold-free aggregates and their subsequent transfer to stirred tank bioreactors, which are ideal for large-scale production and process control. Measuring the growth area of microspheres and aggregates indicated an increasing trend in tissue size in both platforms, consistent with previous reports for aggregates [43] and microspheres [37]. The microsphere platform demonstrated a degree of temporary area uniformity between batches, particularly during the critical initial differentiation stages encompassing CHIR and IWP2 incubation (Fig. 3B and C). This uniformity holds the potential for enhancing batch-to-batch consistency within this platform. While both platforms showed a decline in cell numbers from day −3 to day 0 prior to initiation of differentiation, a substantial increase was noted by day 5, consistent with earlier reports [43]. Although cell numbers decreased after day 5 on both platforms, the decline was less pronounced in the microsphere platform. Further research is needed to understand this cell loss.

Notably, the microspheres not only produced a higher total cell count and percentage of CMs but also yielded a greater number of CMs per initial hiPSC (Fig. 3D and E; Fig. 4A and B). The CM/input hiPSC ratios that we observed in the aggregate platform are consistent with previous studies showing CM/input hPSC ratios of 0.72–0.9 in the aggregate platform [31] and 1–1.25 in another study [71]. While exploring different platforms for aggregate seeding and differentiation (F, P, F/P), no significant differences were observed in terms of CM content and CM yield (Supplementary Figs. 4D and E). This suggests that the platform choice for aggregate method did not significantly impact the overall cardiomyocyte generation across these variations. For the second hiPSC line (IMR90), while a higher number of cells on day 10 compared to the initial hiPSC count was achieved in the microsphere platform—consistent with the original hiPSC line—the percentage change was lower (n = 2 individual batches) (Supplementary Fig. 3). This observation suggests that further optimization may be necessary for each cell line to achieve a higher yield of cell production. Overall, the microsphere platforms consistently demonstrated a higher efficiency in CM differentiation compared to the aggregate, across multiple hiPSC lines.

In addition to examining cellular composition, we investigated post-differentiation characteristics of microsphere and aggregate-derived hiPSC-CMs. Notably, microspheres facilitated intercellular connectivity with prominent Cx43 presence at junctions, enhancing synchronized cardiac function. The even dispersion of mitochondria in microsphere-derived tissues indicated efficient energy distribution. Conversely, aggregates exhibited mitochondria primarily near nuclei, potentially impacting cellular energy dynamics. Further investigation is needed to reveal the corresponding mechanism related to this observation. Remarkably, hiPSC-CMs derived from the microsphere platform demonstrated a significant increase in cell area over time, aligning with the developmental growth in CM size during heart maturation [61] (Fig. 4D). This suggests enhanced cellular maturation within the microsphere platform. Moreover, these cells had significantly larger

areas compared to those from aggregates, highlighting the impact of encapsulation on cellular morphogenesis. However, other morphological parameters, such as cell elongation and circularity, were statistically similar between the two platforms (Fig. 4F–H). The sarcomere length of hiPSC-CMs significantly increased on the microsphere platform compared to the aggregate platform (Fig. 4I). The sarcomere length seen in hiPSC-CMs using the microsphere platform is more similar to the sarcomere length of adult human cardiomyocytes [72].

The comparison of myocardial contractility between the two platforms revealed enhanced contractility in microspheres, even while maintaining a similar average CM content on day 10. The contraction and relaxation velocities measured in the aggregate platform align with prior studies [73]. Microspheres exhibited significantly faster contraction and relaxation velocities compared to aggregates across both hiPSC lines. However, the spontaneous contraction frequency varied between cell lines for the aggregates; for IMR90, aggregates had a significantly lower contraction frequency than microspheres, while Un-Arc 16 Facs II line showed a significantly higher frequency in aggregates compared to microspheres. The contraction frequency was similar between lines for the microspheres. This suggests that contraction frequency may be cell line-dependent, particularly within the aggregate platform (since observed higher variability across hiPSC lines for aggregate) (Supplementary Movies 1-4). Furthermore, the enhanced contraction and relaxation velocities observed over time in microspheres, but not aggregates, suggest that the microsphere platform may offer superior functional performance, particularly with extended culture periods. Moreover, the drug study results suggest a more mature β-adrenergic signaling response in ECTs derived from the microsphere platform (Fig. 6A–D), adding another layer of functional maturity to the characterization of microsphere-derived hiPSC-CMs.

The enhanced contractile functionality observed in the microspheres, as compared to the aggregate, may be attributed to the increased expression of genes involved in the regulation of sarcomeric calcium, such as RYR2 (log2 fc = 1.03 and log p-value = 14.3) and CACNA1 (log2 fc = 0.99 and log p-value = 5), as well as structural proteins of the contractile apparatus [74], [including DMD (log2 fc = 1.16 and log p-value = 8.22), TTN (log2 fc = 2.1 and log p-value = 276), OBSCN (log2 fc = 1.45 and log p-value = 28.9), and DES (log2 fc = 1.18 and log p-value = 5.6) (Fig. 7F). In addition, the sustained activation of the Wnt signaling pathway in the microsphere environment has the potential to facilitate more efficient lineage commitment and differentiation [75].

The differential expression of crucial regulatory genes such as Delta-like 1 homolog (DLK1) and H19 demonstrated differences in microsphere and aggregate platforms during cardiac development and maturation. Interestingly, DLK1, which is expressed in many types of the immature cells [76], was one of the highly expressed genes in the aggregate platform compared to the microsphere platform on day 15. Moreover, the dynamic patterns of H19 expression differed for microspheres versus aggregates. On day 5, the microsphere platform showed relatively higher H19 expression compared to the aggregate platform, indicating a suppression of let-7 micro-RNAs, known for their role in promoting cardiac maturation [62]. At this time, the inhibition may be helpful since it slows down maturation, which means that cardiac precursor cell populations may continue expanding and developing. By day 15, as differentiation progresses towards maturation, the relatively lower H19 expression observed in the microsphere platform suggests a release of inhibition on let-7 micro-RNAs, which likely facilitates the maturation process, as evidenced by the larger cell areas and sarcomere length (Fig. 4), and enhanced contractile velocities (Fig. 5) observed in the microsphere platform. These results suggest a potential regulatory role for H19 in cardiac development and maturation. Further studies may be warranted to fully understand these relationships and their potential to be leveraged in scalable production of hiPSC-derived CMs.

Further to this, increased activities of gene signaling pathways related to cellular structure—including actin cytoskeleton signaling and cardiac hypertrophy signaling—and those related to cell function—such as cardiac conduction and calcium signaling—further confirmed the enhanced cell-cell and cell-matrix interactions in microspheres. This may in turn promote differentiation and maturation more efficiently. Taken together, the transcriptomic data suggests that both molecular and external factors contribute to the improved differentiation and maturation observed in the microsphere platform.

The aggregate system provides simplicity in its approach, requiring minimal additional handling steps beyond initial cell seeding, making it relatively straightforward to implement. Additionally, aggregates require no materials compared to microspheres, which can simplify experimental setups and reduce costs. While microsphere encapsulation offers precise control over cell density within the hydrogel matrix and enables customization of initial size and shape, implementing a microfluidic encapsulation setup requires meticulous adjustments prior to use. These adjustments include optimizing the distance of the light source to the PDMS mold and fine-tuning flow rates to achieve precise spheroid formation. Additionally, there are limitations in the diameter size range of microspheres, which can pose challenges in adjusting these parameters uniformly. The variability in these adjustment parameters across laboratories could lead to differences in results, highlighting the need for standardized protocols and rigorous optimization procedures. It is worth noting that the use of CDM3 for cardiac differentiation may present challenges when compared to traditional B27-supplemented media. In our observations, we noticed higher batch-to-batch variability in hiPSC-CM content and lower contractile functionality during long-term culturing with CDM3 than in our prior work with B27 [37]. Ongoing research into CDM3 formulation may overcome the variability that was observed here, based on work by Kriedemann and Zweigerdt et al. (unpublished). Our findings underscore the potential limitations of CDM3 and emphasize the importance of this further investigation and optimization to ensure consistent and robust differentiation outcomes in cardiac tissue engineering applications.

In summary, this direct comparative assessment of cardiac microspheres and aggregates has offered valuable insights into the distinct capabilities of these two systems in terms of cell production, contractile functionality, and structural maturation attributes. These collective findings enrich understanding of the potential impact of encapsulation strategies prior to hiPSC differentiation on cardiomyocyte structural maturation, offering pathways for tailored optimization of cardiac tissue engineering. Further research is needed to uncover the underlying molecular mechanisms and signaling pathways that drive these observed differences, alongside an exploration of their implications within regenerative medicine and disease modeling. Results of this study substantiate the potential of microspheres as a platform to propel advancements in cardiac tissue engineering strategies and contribute to a deeper grasp of their applicability in regenerative medicine contexts.

5. Conclusions

This study presents an exploration of the differentiation potential and contractile functionality attributes of cardiac microspheres and aggregates, shedding light on their distinct characteristics and providing insights into implications of platform selection on cardiac tissue engineering. Utilizing scaffold-supported (microsphere) and scaffold-free (aggregate) techniques, hiPSC-CMs were generated within a suspension-based culture platform under chemically defined conditions suitable for scalable production. The incorporation of PF hydrogel as a 3D microenvironment for hiPSCs facilitated both encapsulation and differentiation, resulting in significant differences in cell production, cardiac differentiation, contractile functionality, structural maturation of the resulting hiPSC-CMs, and responses to pharmacological stimulation.

Microspheres exhibited a notably higher percentage of CMs, along with a greater CM yield compared to aggregates, indicating a superior capacity for cardiomyogenic differentiation. The scaffold-supported

(microsphere) technique demonstrated improvements in contractile functionality, β-adrenergic signaling response, and cell and sarcomere morphologies, underscoring its capabilities in cardiac differentiation and engineered cardiac tissues (ECTs) production. These findings were corroborated by transcriptomic analysis, which revealed that while both microsphere and aggregate platforms demonstrated similar gene regulation patterns associated with cardiomyocyte differentiation, heart development, cardiac muscle contraction, and sarcomere organization, the microsphere platform exhibited more pronounced transcriptional changes over time. However, a deeper understanding of the underlying molecular mechanisms for use of these ECTs in disease modeling and clinical translation is warranted. This research provides valuable insights for tailoring approaches to optimize cardiac tissue engineering, emphasizing the promise of microspheres in hiPSC-CM production and maturation.

Ethics approval and consent to participate

This research is not related to clinical study and this research did not involve experimentation on animals or humans.

Data availability

The raw data required to reproduce these findings are available upon request. The RNAseq data set generated in this study (GSE276741) is available from the NCBI Gene Expression Omnibus database (https://www.ncbi.nlm.nih.gov/geo/query/acc.cgi?acc=GSE276741).

CRediT authorship contribution statement

Mohammadjafar Hashemi: Writing – original draft, Methodology, Investigation, Formal analysis, Data curation, Conceptualization. **Ferdous B. Finklea:** Validation, Methodology, Data curation, Conceptualization. **Hanna Hammons:** Data curation. **Yuan Tian:** Writing – review & editing, Conceptualization. **Nathan Young:** Formal analysis. **Emma Kim:** Formal analysis. **Caroline Halloin:** Methodology. **Wiebke Triebert:** Methodology. **Robert Zweigerdt:** Conceptualization. **Amit Kumar Mitra:** Formal analysis, Validation, Writing – review & editing. **Elizabeth A. Lipke:** Writing – review & editing, Validation, Supervision, Resources, Methodology, Investigation, Conceptualization.

Declaration of Competing Interest

Auburn University holds four patents related to the cardiac differentiation approach and the microfluidic cell encapsulation system employed in this manuscript.

Acknowledgements

This work was funded by the National Science Foundation (NSFCBET-1150854 and 2135059) (E.A.L.), an American Heart Association (916440) Pre-doctoral Fellowship (M.H.), and an NSF Graduate Research Fellowship (F.B.F.). This work was supported by the following funds to (R.Z.): German Research Foundation (DFG; grants: Cluster of Excellence REBIRTH EXC 62/2, ZW 64/4-2), Federal Ministry of Education and Research (BMBF, grants: 01EK1601A, 031L0249, 01EK2108A), Lower Saxony ("Förderung aus Mitteln des Niedersächsischen Vorab" and „Zukunft Niedersachsen“; grants: ZN3340, ZN4092), and the European Union, EU Horizon, project HEAL, contract 101056712. Views and opinions expressed are however those of the author(s) only and do not necessarily reflect those of the European Union or the European Health and Digital Executive Agency (HADEA). Neither the European Union nor the granting authority can be held responsible for them. The authors gratefully acknowledge Dr. Saucerman for the providing unbiased algorithm and sharing their MATLAB code with us for analyzing the confocal images. The authors appreciate B. Justin Harvell for conducting the final proofreading. Schematic figure created using biorender.com.

Appendix A. Supplementary data

Supplementary data to this article can be found online at https://doi.org/10.1016/j.bioactmat.2024.08.043.

Abbreviation

2D	Two-dimensional
3D	Three-dimensional
αSA	α-sarcomeric actinin
ABS	Acrylonitrile butadiene styrene
Agg	Aggregates
ANOVA	Analysis of variance
AR	Axial ratio
BSA	Bovine serum albumin
CDM3	Chemically defined medium containing three components
CM	Cardiomyocyte
CoV	Coefficient of variation
CPM	Counts per million
cTnT	Cardiac troponin T
CTD50	Calcium transient durations at 50 %
CTD80	Calcium transient durations at 80 %
CV	Conduction velocity
Cx43	Connexin 43
DE	Differential expression
DEGs	Differentially expressed genes
DLK1	Delta-like 1 homolog
ECT	Engineered cardiac tissue
ECM	Extracellular matrix
ESCs	Embryonic stem cells
F/P	Hybrid approach involving seeding in a shaker flask and subsequent differentiation within a well plate
F	Seeding and differentiation within a shaker flask
FBS	Fetal bovine serum
GEP	Gene expression profiling
GO	Gene ontologies
GSA	Gene-specific analysis
GSEA	Gene set enrichment analysis
HC	Unsupervised hierarchical clustering
hiPSC-CMs	hiPSC-derived CMs
hiPSCs	Human induced pluripotent stem cells
ILK	Integrin-linked kinase
IPA	Ingenuity pathway analysis
Iso	Isoproterenol
KCl	Potassium chloride
LS	Least squares
MS	Microspheres
MYOM1	Myomesin-1
NES	Normalized enrichment scores
NVP	N-vinylpyrrolidone
P	Seeding and differentiation within a well plate
PBS	Phosphate buffered saline
PDMS	Polydimethylsiloxane
PFA	Paraformaldehyde
PF	PEG-fibrinogen
PEG-fibrinogen	Poly(ethylene glycol)-fibrinogen
PEGDA	Poly(ethylene glycol)-diacrylate
Pro	Propranolol
RI	ROCK inhibitor
RIN	RNA integrity number
ROUT	Robust regression and outlier removal
SOTA	SarcOmere texture analysis
SD	Standard deviation

TCEP-HCl Tris (2-carboxyethyl) phosphine hydrochloride
TEOA Triethanolamine

References

[1] G. Campostrini, L.M. Windt, B.J. van Meer, M. Bellin, C.L. Mummery, Cardiac tissues from stem cells: new routes to maturation and cardiac regeneration, Circ. Res. 128 (2021) 775–801, https://doi.org/10.1161/CIRCRESAHA.121.318183.

[2] N.T. Feric, M. Radisic, Towards adult-like human engineered cardiac tissue: maturing human pluripotent stem cell-derived cardiomyocytes in human engineered cardiac tissues, Adv. Drug Deliv. Rev. 96 (2016) 110, https://doi.org/10.1016/j.addr.2015.04.019.

[3] M.E. Kupfer, W.H. Lin, V. Ravikumar, K. Qiu, L. Wang, L. Gao, D.B. Bhuiyan, M. Lenz, J. Ai, R.R. Mahutga, D. Townsend, J. Zhang, M.C. McAlpine, E. G. Tolkacheva, B.M. Ogle, In situ expansion, differentiation, and electromechanical coupling of human cardiac muscle in a 3D bioprinted, chambered organoid, Circ. Res. 127 (2020) 207–224, https://doi.org/10.1161/CIRCRESAHA.119.316155.

[4] G.V. Novakovic, T. Eschenhagen, C. Mummery, Myocardial tissue engineering: in vitro models, Cold Spring Harbor Perspectives in Medicine 4 (2014) a014076, https://doi.org/10.1101/cshperspect.a014076.

[5] Y. Kishino, J. Fujita, S. Tohyama, M. Okada, S. Tanosaki, S. Someya, K. Fukuda, Toward the realization of cardiac regenerative medicine using pluripotent stem cells, Inflamm. Regen. 40 (2020) 1, https://doi.org/10.1186/s41232-019-0110-4.

[6] V.C. Chen, J. Ye, P. Shukla, G. Hua, D. Chen, Z. Lin, J.C. Liu, J. Chai, J. Gold, J. Wu, D. Hsu, L.A. Couture, Development of a scalable suspension culture for cardiac differentiation from human pluripotent stem cells, Stem Cell Res. 15 (2015) 365–375, https://doi.org/10.1016/j.scr.2015.08.002.

[7] A. Chen, S. Ting, J. Seow, S. Reuveny, S. Oh, Considerations in designing systems for large scale production of human cardiomyocytes from pluripotent stem cells, Stem Cell Res. Ther. 5 (2014) 12, https://doi.org/10.1186/scrt401.

[8] G.J. Scuderi, J. Butcher, Naturally engineered maturation of cardiomyocytes, Front. Cell Dev. Biol. 5 (2017) 50, https://doi.org/10.3389/fcell.2017.00050.

[9] K. Ban, S. Bae, Y.S. Yoon, Current strategies and challenges for purification of cardiomyocytes derived from human pluripotent stem cells, Theranostics 7 (2017) 2067–2077, https://doi.org/10.7150/thno.19427.

[10] N. Chanthra, T. Abe, M. Miyamoto, K. Sekiguchi, C. Kwon, Y. Hanazono, H. Uosaki, A novel fluorescent reporter system identifies laminin-511/521 as potent regulators of cardiomyocyte maturation, Sci. Rep. 10 (2020) 1–13, https://doi.org/10.1038/s41598-020-61163-3.

[11] D. Thomas, N.J. Cunningham, S. Shenoy, J.C. Wu, Human-induced pluripotent stem cells in cardiovascular research: current approaches in cardiac differentiation, maturation strategies, and scalable production, Cardiovasc. Res. 118 (2022) 20–36, https://doi.org/10.1093/cvr/cvab115.

[12] C. Correia, A. Koshkin, P. Duarte, D. Hu, M. Carido, M.J. Sebastiao, P. Gomes-Alves, D.A. Elliott, I.J. Domian, A.P. Teixeira, P.M. Alves, M. Serra, 3D aggregate culture improves metabolic maturation of human pluripotent stem cell derived cardiomyocytes, Biotechnol. Bioeng. 115 (2018) 630–644, https://doi.org/10.1002/bit.26504.

[13] Y. Haraguchi, K. Matsuura, T. Shimizu, M. Yamato, T. Okano, Simple suspension culture system of human iPS cells maintaining their pluripotency for cardiac cell sheet engineering, Journal of Tissue Engineering and Regenerative Medicine 9 (2015) 1363–1375, https://doi.org/10.1002/term.1761.

[14] H. Kempf, B. Andree, R. Zweigerdt, Large-scale production of human pluripotent stem cell derived cardiomyocytes, Adv. Drug Deliv. Rev. 96 (2016) 18–30, https://doi.org/10.1016/j.addr.2015.11.016.

[15] C.K. Kwok, I. Sebastien, K. Hariharan, I. Meiser, J. Wihan, S. Altmaier, I. Karnatz, D. Bauer, B. Fischer, A. Feile, A. Cabrera-Socorro, M. Rasmussen, B. Holst, J. C. Neubauer, C. Clausen, C. Verfaillie, A. Ebneth, M. Hansson, R. Steeg, H. Zimmermann, Scalable expansion of iPSC and their derivatives across multiple lineages, Reprod. Toxicol. 112 (2022) 23–35, https://doi.org/10.1016/j.reprotox.2022.05.007.

[16] P. Beauchamp, W. Moritz, J.M. Kelm, N.D. Ullrich, I. Agarkova, B.D. Anson, T. M. Suter, C. Zuppinger, Development and characterization of a scaffold-free 3D spheroid model of induced pluripotent stem cell-derived human cardiomyocytes, Tissue Eng Part C Methods 21 (2015) 852–861, https://doi.org/10.1089/ten.TEC.2014.0376.

[17] S. Breslin, L. O'Driscoll, Three-dimensional cell culture: the missing link in drug discovery, Drug Discov. Today 18 (2013) 240–249, https://doi.org/10.1016/j.drudis.2012.10.003.

[18] M.A. Branco, J.P. Cotovio, C.A.V. Rodrigues, S.H. Vaz, T.G. Fernandes, L. M. Moreira, J.M.S. Cabral, M.M. Diogo, Transcriptomic analysis of 3D cardiac differentiation of human induced pluripotent stem cells reveals faster cardiomyocyte maturation compared to 2D culture, Sci. Rep. 9 (2019) 9229, https://doi.org/10.1038/s41598-019-45047-9.

[19] S. Ting, A. Chen, S. Reuveny, S. Oh, An intermittent rocking platform for integrated expansion and differentiation of human pluripotent stem cells to cardiomyocytes in suspended microcarrier cultures, Stem Cell Res. 13 (2014) 202–213, https://doi.org/10.1016/j.scr.2014.06.002.

[20] F. Laco, A.T. Lam, T.L. Woo, G. Tong, V. Ho, P.L. Soong, E. Grishina, K.H. Lin, S. Reuveny, S.K. Oh, Selection of human induced pluripotent stem cells lines optimization of cardiomyocytes differentiation in an integrated suspension microcarrier bioreactor, Stem Cell Res. Ther. 11 (2020) 118, https://doi.org/10.1186/s13287-020-01618-6.

[21] M. Lecina, S. Ting, A. Choo, S. Reuveny, S. Oh, Scalable platform for human embryonic stem cell differentiation to cardiomyocytes in suspended microcarrier cultures, Tissue Eng Part C Methods 16 (2010) 1609–1619, https://doi.org/10.1089/ten.TEC.2010.0104.

[22] A.M. Martins, G. Eng, S.G. Caridade, J.F. Mano, R.L. Reis, G. Vunjak-Novakovic, Electrically conductive chitosan/carbon scaffolds for cardiac tissue engineering, Biomacromolecules 15 (2014) 635–643, https://doi.org/10.1021/bm401679q.

[23] H. Park, B.L. Larson, M.E. Kolewe, G. Vunjak-Novakovic, L.E. Freed, Biomimetic scaffold combined with electrical stimulation and growth factor promotes tissue engineered cardiac development, Exp. Cell Res. 321 (2014) 297–306, https://doi.org/10.1016/j.yexcr.2013.11.005.

[24] S.B. Seif-Naraghi, J.M. Singelyn, M.A. Salvatore, K.G. Osborn, J.J. Wang, U. Sampat, O.L. Kwan, G.M. Strachan, J. Wong, P.J. Schup-Magoffin, R.L. Braden, K. Bartels, J.A. DeQuach, M. Preul, A.M. Kinsey, A.N. DeMaria, N. Dib, K. L. Christman, Safety and efficacy of an injectable extracellular matrix hydrogel for treating myocardial infarction, Sci. Transl. Med. 5 (2013) 173ra25, https://doi.org/10.1126/scitranslmed.3005503.

[25] S.M. Willerth, S.E. Sakiyama-Elbert, Combining stem cells and biomaterial scaffolds for constructing tissues and cell delivery, StemJournal 1 (2019) 1–25, https://doi.org/10.3233/STJ-180001.

[26] A. Ovsianikov, A. Khademhosseini, V. Mironov, The synergy of scaffold-based and scaffold-free tissue engineering strategies, Trends Biotechnol. 36 (2018) 348–357, https://doi.org/10.1016/j.tibtech.2018.01.005.

[27] M.A. Kinney, C.Y. Sargent, T.C. McDevitt, The multiparametric effects of hydrodynamic environments on stem cell culture, Tissue Eng Part B Rev 17 (2011) 249–262, https://doi.org/10.1089/ten.TEB.2011.0040.

[28] M.A. Kinney, T.A. Hookway, Y. Wang, T.C. McDevitt, Engineering three-dimensional stem cell morphogenesis for the development of tissue models and scalable regenerative therapeutics, Ann. Biomed. Eng. 42 (2014) 352–367, https://doi.org/10.1007/s10439-013-0953-9.

[29] A.W. Xie, B.Y.K. Binder, A.S. Khalil, S.K. Schmitt, H.J. Johnson, N.A. Zacharias, W. L. Murphy, Controlled self-assembly of stem cell aggregates instructs pluripotency and lineage bias, Sci. Rep. 7 (2017) 14070, https://doi.org/10.1038/s41598-017-14325-9.

[30] K. Osafune, L. Caron, M. Borowiak, R.J. Martinez, C.S. Fitz-Gerald, Y. Sato, C. A. Cowan, K.R. Chien, D.A. Melton, Marked differences in differentiation propensity among human embryonic stem cell lines, Nat. Biotechnol. 26 (2008) 313–315, https://doi.org/10.1038/nbt1383.

[31] H. Kempf, R. Olmer, C. Kropp, M. Ruckert, M. Jara-Avaca, D. Robles-Diaz, A. Franke, D.A. Elliott, D. Wojciechowski, M. Fischer, A. Roa Lara, G. Kensah, I. Gruh, A. Haverich, U. Martin, R. Zweigerdt, Controlling expansion and cardiomyogenic differentiation of human pluripotent stem cells in scalable suspension culture, Stem Cell Rep. 3 (2014) 1132–1146, https://doi.org/10.1016/j.stemcr.2014.09.017.

[32] C.L. Bauwens, D. Toms, M. Ungrin, Aggregate size optimization in microwells for suspension-based cardiac differentiation of human pluripotent stem cells, J. Vis. Exp. (2016) e54308, https://doi.org/10.3791/54308.

[33] F.G. Torizal, S.M. Kim, I. Horiguchi, K. Inamura, I. Suzuki, T. Morimura, M. Nishikawa, Y. Sakai, Production of homogenous size-controlled human induced pluripotent stem cell aggregates using ring-shaped culture vessel, J Tissue Eng Regen Med 16 (2022) 254–266, https://doi.org/10.1002/term.3278.

[34] S. Niebruegge, C.L. Bauwens, R. Peerani, N. Thavandiran, S. Masse, E. Sevaptisidis, K. Nanthakumar, K. Woodhouse, M. Husain, E. Kumacheva, P.W. Zandstra, Generation of human embryonic stem cell-derived mesoderm and cardiac cells using size-specified aggregates in an oxygen-controlled bioreactor, Biotechnol. Bioeng. 102 (2009) 493–507, https://doi.org/10.1002/bit.22065.

[35] P. Gupta, M.Z. Ismadi, P.J. Verma, A. Fouras, S. Jadhav, J. Bellare, K. Hourigan, Optimization of agitation speed in spinner flask for microcarrier structural integrity and expansion of induced pluripotent stem cells, Cytotechnology 68 (2016) 45–59, https://doi.org/10.1007/s10616-014-9750-z.

[36] D. Sridharan, A. Palaniappan, B.N. Blackstone, J.A. Dougherty, N. Kumar, P. B. Seshagiri, N. Sayed, H.M. Powell, M. Khan, In situ differentiation of human-induced pluripotent stem cells into functional cardiomyocytes on a coaxial PCL-gelatin nanofibrous scaffold, Mater. Sci. Eng., C 118 (2021) 111354, https://doi.org/10.1016/j.msec.2020.111354.

[37] F.B. Finklea, Y. Tian, P. Kerscher, W.J. Seeto, M.E. Ellis, E.A. Lipke, Engineered cardiac tissue microsphere production through direct differentiation of hydrogel-encapsulated human pluripotent stem cells, Biomaterials 274 (2021) 120818, https://doi.org/10.1016/j.biomaterials.2021.120818.

[38] M.E. Ellis, B.N. Harris, M. Hashemi, B.J. Harvell, M.Z. Bush, E.E. Hicks, F. B. Finklea, E.M. Wang, R. Nataraj, N.P. Young, I.C. Turnbull, E.A. Lipke, Human induced pluripotent stem cell encapsulation geometry impacts three-dimensional developing human engineered cardiac tissue functionality, Tissue Eng Part A 28 (2022) 990–1000, https://doi.org/10.1089/ten.TEA.2022.0107.

[39] S. Chang, F. Finklea, B. Williams, H. Hammons, A. Hodge, S. Scott, E. Lipke, Emulsion-based encapsulation of pluripotent stem cells in hydrogel microspheres for cardiac differentiation, Biotechnol. Prog. 36 (2020) e2986, https://doi.org/10.1002/btpr.2986.

[40] P. Kerscher, J.A. Kaczmarek, S.E. Head, M.E. Ellis, W.J. Seeto, J. Kim, S. Bhattacharya, V. Suppiramaniam, E.A. Lipke, Direct production of human cardiac tissues by pluripotent stem cell encapsulation in gelatin methacryloyl, ACS Biomater. Sci. Eng. 3 (2017) 1499–1509, https://doi.org/10.1021/acsbiomaterials.6b00226.

[41] D. Jing, A. Parikh, E.S. Tzanakakis, Cardiac cell generation from encapsulated embryonic stem cells in static and scalable culture systems, Cell Transplant. 19 (2010) 1397–1412, https://doi.org/10.3727/096368910X513955.

[42] W.J. Seeto, Y. Tian, S. Pradhan, P. Kerscher, E.A. Lipke, Rapid production of cell-laden microspheres using a flexible microfluidic encapsulation platform, Small 15 (2019) e1902058, https://doi.org/10.1002/smll.201902058.
[43] C. Halloin, K. Schwanke, W. Löbel, A. Franke, M. Szepes, S. Biswanath, S. Wunderlich, S. Merkert, N. Weber, F. Osten, Continuous WNT control enables advanced hPSC cardiac processing and prognostic surface marker identification in chemically defined suspension culture, Stem Cell Rep. 13 (2019) 366–379, https://doi.org/10.1016/j.stemcr.2019.09.001.
[44] R. Shinnawi, I. Huber, L. Maizels, N. Shaheen, A. Gepstein, G. Arbel, A.J. Tijsen, L. Gepstein, Monitoring human-induced pluripotent stem cell-derived cardiomyocytes with genetically encoded calcium and voltage fluorescent reporters, Stem Cell Rep. 5 (2015) 582–596, https://doi.org/10.1016/j.stemcr.2015.08.009.
[45] H. Kempf, C. Kropp, R. Olmer, U. Martin, R. Zweigerdt, Cardiac differentiation of human pluripotent stem cells in scalable suspension culture, Nat. Protoc. 10 (2015) 1345–1361, https://doi.org/10.1038/nprot.2015.089.
[46] S.A. DeLong, J.J. Moon, J.L. West, Covalently immobilized gradients of bFGF on hydrogel scaffolds for directed cell migration, Biomaterials 26 (2005) 3227–3234, https://doi.org/10.1016/j.biomaterials.2004.09.021.
[47] S. Trattnig, K. Ohel, V. Mlynarik, V. Juras, S. Zbyn, A. Korner, Morphological and compositional monitoring of a new cell-free cartilage repair hydrogel technology - GelrinC by MR using semi-quantitative MOCART scoring and quantitative T2 index and new zonal T2 index calculation, Osteoarthritis Cartilage 23 (2015) 2224–2232, https://doi.org/10.1016/j.joca.2015.07.007.
[48] M. Plotkin, S.R. Vaibavi, A.J. Rufaihah, V. Nithya, J. Wang, Y. Shachaf, T. Kofidis, D. Seliktar, The effect of matrix stiffness of injectable hydrogels on the preservation of cardiac function after a heart attack, Biomaterials 35 (2014) 1429–1438, https://doi.org/10.1016/j.biomaterials.2013.10.058.
[49] L. Almany, D. Seliktar, Biosynthetic hydrogel scaffolds made from fibrinogen and polyethylene glycol for 3D cell cultures, Biomaterials 26 (2005) 2467–2477, https://doi.org/10.1016/j.biomaterials.2004.06.047.
[50] N. Kriedemann, W. Triebert, J. Teske, M. Mertens, A. Franke, K. Ullmann, F. Manstein, L. Drakhlis, A. Haase, C. Halloin, U. Martin, R. Zweigerdt, Standardized production of hPSC-derived cardiomyocyte aggregates in stirred spinner flasks, Nat. Protoc. (2024) 1–29, https://doi.org/10.1038/s41596-024-00976-2.
[51] P.W. Burridge, E. Matsa, P. Shukla, Z.C. Lin, J.M. Churko, A.D. Ebert, F. Lan, S. Diecke, B. Huber, N.M. Mordwinkin, J.R. Plews, O.J. Abilez, B. Cui, J.D. Gold, J. C. Wu, Chemically defined generation of human cardiomyocytes, Nat. Methods 11 (2014) 855–860, https://doi.org/10.1038/nmeth.2999.
[52] M.D. Sutcliffe, P.M. Tan, A. Fernandez-Perez, Y.J. Nam, N.V. Munshi, J. J. Saucerman, High content analysis identifies unique morphological features of reprogrammed cardiomyocytes, Sci. Rep. 8 (2018) 1258, https://doi.org/10.1038/s41598-018-19539-z.
[53] C.N. Toepfer, A. Sharma, M. Cicconet, A.C. Garfinkel, M. Mücke, M. Neyazi, J.A. L. Willcox, R. Agarwal, M. Schmid, J. Rao, J. Eweldt, O. Pourquié, A. Chopra, C. S. Chen, J.G. Seidman, C.E. Seidman, SarcTrack an adaptable software tool for efficient large-scale analysis of sarcomere function in hiPSC-cardiomyocytes, Circ. Res. 124 (2019) 1172–1183, https://doi.org/10.1161/Circresaha.118.314505.
[54] P. Kerscher, B.S. Bussie, K.M. DeSimone, D.A. Dunn, E.A. Lipke, Characterization of mitochondrial populations during stem cell differentiation, in: Mitochondrial Medicine, Springer, 2015, pp. 453–463, https://doi.org/10.1007/978-1-4939-2257-4_37.
[55] N. Huebsch, P. Loskill, M.A. Mandegar, N.C. Marks, A.S. Sheehan, Z. Ma, A. Mathur, T.N. Nguyen, J.C. Yoo, L.M. Judge, C.I. Spencer, A.C. Chukka, C. R. Russell, P.L. So, B.R. Conklin, K.E. Healy, Automated video-based analysis of contractility and calcium flux in human-induced pluripotent stem cell-derived cardiomyocytes cultured over different spatial scales, Tissue Eng Part C Methods 21 (2015) 467–479, https://doi.org/10.1089/ten.TEC.2014.0283.
[56] A.J. Hodge, J. Zhong, E.A. Lipke, Enhanced stem cell-derived cardiomyocyte differentiation in suspension culture by delivery of nitric oxide using S-nitrosocysteine, Biotechnol. Bioeng. 113 (2016) 882–894, https://doi.org/10.1002/bit.25849.
[57] S. Mazumder, T. Mitra Ghosh, U.K. Mukherjee, S. Chakravarti, F. Amiri, R. S. Waliagha, F. Hemmati, P. Mistriotis, S. Ahmed, I. Elhussin, A.B. Salam, W. Dean-Colomb, C. Yates, R.D. Arnold, A.K. Mitra, Integrating pharmacogenomics data-driven computational drug prediction with single-cell RNAseq to demonstrate the efficacy of a NAMPT inhibitor against aggressive, taxane-resistant, and stem-like cells in lethal prostate cancer, Cancers 14 (2022), https://doi.org/10.3390/cancers14236009.
[58] A. Krämer, J. Green, J. Pollard, S. Tugendreich, Causal analysis approaches in Ingenuity Pathway Analysis 30 (2014) 523–530, https://doi.org/10.1093/bioinformatics/btt703.
[59] A. Subramanian, P. Tamayo, V.K. Mootha, S. Mukherjee, B.L. Ebert, M.A. Gillette, A. Paulovich, S.L. Pomeroy, T.R. Golub, E.S. Lander, J.P. Mesirov, Gene set enrichment analysis: a knowledge-based approach for interpreting genome-wide expression profiles, Proc Natl Acad Sci U S A 102 (2005) 15545–15550, https://doi.org/10.1073/pnas.0506580102.
[60] J.M. Brickman, P. Serup, Properties of embryoid bodies, Wiley Interdiscip Rev Dev Biol 6 (2017) e259, https://doi.org/10.1002/wdev.259.
[61] I. Shimizu, T. Minamino, Physiological and pathological cardiac hypertrophy, J. Mol. Cell. Cardiol. 97 (2016) 245–262, https://doi.org/10.1016/j.yjmcc.2016.06.001.
[62] T. Grancharova, K.A. Gerbin, A.B. Rosenberg, C.M. Roco, J.E. Arakaki, C. M. DeLizo, S.Q. Dinh, R.M. Donovan-Maiye, M. Hirano, A.M. Nelson, A comprehensive analysis of gene expression changes in a high replicate and open-source dataset of differentiating hiPSC-derived cardiomyocytes, Sci. Rep. 11 (2021) 15845, https://doi.org/10.1038/s41598-021-94732-1.
[63] C. Fuoco, M.L. Salvatori, A. Biondo, K. Shapira-Schweitzer, S. Santoleri, S. Antonini, S. Bernardini, F.S. Tedesco, S. Cannata, D. Seliktar, G. Cossu, C. Gargioli, Injectable polyethylene glycol-fibrinogen hydrogel adjuvant improves survival and differentiation of transplanted mesoangioblasts in acute and chronic skeletal-muscle degeneration, Skelet Muscle 2 (2012) 24, https://doi.org/10.1186/2044-5040-2-24.
[64] P. Kerscher, I.C. Turnbull, A.J. Hodge, J. Kim, D. Seliktar, C.J. Easley, K.D. Costa, E. A. Lipke, Direct hydrogel encapsulation of pluripotent stem cells enables ontomimetic differentiation and growth of engineered human heart tissues, Biomaterials 83 (2016) 383–395, https://doi.org/10.1016/j.biomaterials.2015.12.011.
[65] B.S. Borys, A. Le, E.L. Roberts, T. Dang, L. Rohani, C.Y. Hsu, A.A. Wyma, D. E. Rancourt, I.D. Gates, M.S. Kallos, Using computational fluid dynamics (CFD) modeling to understand murine embryonic stem cell aggregate size and pluripotency distributions in stirred suspension bioreactors, J. Biotechnol. 304 (2019) 16–27, https://doi.org/10.1016/j.jbiotec.2019.08.002.
[66] T.G. Otsuji, J. Bin, A. Yoshimura, M. Tomura, D. Tateyama, I. Minami, Y. Yoshikawa, K. Aiba, J.E. Heuser, T. Nishino, K. Hasegawa, N. Nakatsuji, A 3D sphere culture system containing functional polymers for large-scale human pluripotent stem cell production, Stem Cell Rep. 2 (2014) 734–745, https://doi.org/10.1016/j.stemcr.2014.03.012.
[67] A. Kahn-Krell, D. Pretorius, J. Ou, V.G. Fast, S. Litovsky, J. Berry, X.M. Liu, J. Zhang, Bioreactor suspension culture: differentiation and production of cardiomyocyte spheroids from human induced pluripotent stem cells, Front. Bioeng. Biotechnol. 9 (2021) 674260, https://doi.org/10.3389/fbioe.2021.674260.
[68] S. Sart, J. Bejoy, Y. Li, Characterization of 3D pluripotent stem cell aggregates and the impact of their properties on bioprocessing, Process Biochemistry 59 (2017) 276–288, https://doi.org/10.1016/j.procbio.2016.05.024.
[69] M. Pesl, I. Acimovic, J. Pribyl, R. Hezova, A. Vilotic, J. Fauconnier, J. Vrbsky, P. Kruzliak, P. Skladal, T. Kara, V. Rotrekl, A. Lacampagne, P. Dvorak, A.C. Meli, Forced aggregation and defined factors allow highly uniform-sized embryoid bodies and functional cardiomyocytes from human embryonic and induced pluripotent stem cells, Heart Ves. 29 (2014) 834–846, https://doi.org/10.1007/s00380-013-0436-9.
[70] M.H. Kim, K. Takeuchi, M. Kino-Oka, Role of cell-secreted extracellular matrix formation in aggregate formation and stability of human induced pluripotent stem cells in suspension culture, J. Biosci. Bioeng. 127 (2019) 372–380, https://doi.org/10.1016/j.jbiosc.2018.08.010.
[71] H. Fonoudi, H. Ansari, S. Abbasalizadeh, M.R. Larijani, S. Kiani, S. Hashemizadeh, A.S. Zarchi, A. Bosman, G.M. Blue, S. Pahlavan, M. Perry, Y. Orr, Y. Mayorchak, J. Vandenberg, M. Talkhabi, D.S. Winlaw, R.P. Harvey, N. Aghdami, H. Baharvand, A universal and robust integrated platform for the scalable production of human cardiomyocytes from pluripotent stem cells, Stem Cells Transl Med 4 (2015) 1482–1494, https://doi.org/10.5966/sctm.2014-0275.
[72] E. Karbassi, A. Fenix, S. Marchiano, N. Muraoka, K. Nakamura, X. Yang, C. E. Murry, Cardiomyocyte maturation: advances in knowledge and implications for regenerative medicine, Nat. Rev. Cardiol. 17 (2020) 341–359, https://doi.org/10.1038/s41569-019-0331-x.
[73] D. Thomas, H. Kim, N. Lopez, J.C. Wu, Fabrication of 3D cardiac microtissue arrays using human iPSC-derived cardiomyocytes, cardiac fibroblasts, and endothelial cells, J. Vis. Exp. (2021) e61879, https://doi.org/10.3791/61879.
[74] E. Ergir, J. Oliver-De La Cruz, S. Fernandes, M. Cassani, F. Niro, D. Pereira-Sousa, J. Vrbský, V. Vinarský, A.R. Perestrelo, D. Debellis, Generation and maturation of human iPSC-derived 3D organotypic cardiac microtissues in long-term culture, Sci. Rep. 12 (2022) 17409, https://doi.org/10.1038/s41598-022-22225-w.
[75] M. Zhao, Y. Tang, Y. Zhou, J. Zhang, Deciphering role of Wnt signalling in cardiac mesoderm and cardiomyocyte differentiation from human iPSCs: four-dimensional control of Wnt pathway for hiPSC-CMs differentiation, Sci. Rep. 9 (2019) 19389, https://doi.org/10.1038/s41598-019-55620-x.
[76] G.Á. Traustadóttir, L.V. Lagoni, L.B.S. Ankerstjerne, H.C. Bisgaard, C.H. Jensen, D. C. Andersen, The imprinted gene Delta like non-canonical Notch ligand 1 (Dlk1) is conserved in mammals, and serves a growth modulatory role during tissue development and regeneration through Notch dependent and independent mechanisms, Cytokine Growth Factor Rev. 46 (2019) 17–27, https://doi.org/10.1016/j.cytogfr.2019.03.006.